



Calhoun: The NPS Institutional Archive
DSpace Repository

Theses and Dissertations

1. Thesis and Dissertation Collection, all items

1955

Instrumentation and calibration of x-ray scintillation pair spectrometer.

Snyder, Joseph Edward

Massachusetts Institute of Technology

<http://hdl.handle.net/10945/14268>

Downloaded from NPS Archive: Calhoun



Calhoun is the Naval Postgraduate School's public access digital repository for research materials and institutional publications created by the NPS community. Calhoun is named for Professor of Mathematics Guy K. Calhoun, NPS's first appointed -- and published -- scholarly author.

Dudley Knox Library / Naval Postgraduate School
411 Dyer Road / 1 University Circle
Monterey, California USA 93943

<http://www.nps.edu/library>

**INSTRUMENTATION AND CALIBRATION OF X-RAY
SCINTILLATION PAIR SPECTROMETER**

Joseph Edward Synder, Jr.

Library
U. S. Naval Postgraduate School
Monterey, California

22211
28222

INSTRUMENTATION AND CALIBRATION OF
X-RAY SCINTILLATION PAIR SPECTROMETER

by

Joseph Edward Snyder, Jr.
B.S., United States Naval Academy
(1944)

Submitted in Partial Fulfillment of the
Requirements for the Degree of

MASTER OF SCIENCE

at the

MASSACHUSETTS INSTITUTE OF TECHNOLOGY
(1955)

Signature of Author _____ Department of Physics, May 23, 1955

Certified by _____ Thesis Supervisor

Accepted by _____ Chairman, Departmental Committee on Graduate Students

56625

INVESTIGATION AND EVALUATION OF
X-RAY FLUORESCENCE ANALYSIS

by

James Edward Taylor, Jr.
U.S. Naval Research Laboratory
(1955)

Submitted in partial fulfillment of the
requirements for the degree of

MASTERS OF SCIENCE

at the

MASSACHUSETTS INSTITUTE OF TECHNOLOGY
(1955)

Signature of Author _____
Department of Physics, May 23, 1957

Certified by _____
Thesis Supervisor

Accepted by _____
Chairman, Departmental Committee on Graduate Students

INSTRUMENTATION AND CALIBRATION OF
X-RAY SCINTILLATION PAIR SPECTROMETER

by

Joseph Edward Snyder, Jr.

Submitted to the Department of Physics on May 23, 1955 in partial fulfillment of the requirements for the degree of Master of Science.

ABSTRACT

This paper describes an x-ray spectrometer designed for use at the M.I.T. linear accelerator. The spectrometer is a three-counter telescope with a thin lead radiator between the first and second counter. The first and second counters are thin plastic scintillators; the third, a thick plastic scintillator. An acceptable event is one in which there is no pulse in the first counter and a doubly ionizing pulse in the second counter in coincidence with the third counter. Such events should be electron-positron pairs originating only in the radiator. To a first approximation, the sum of the pulse heights produced in the second and third counter is proportional to the incident x-ray energy.

Thesis Supervisor: Bernard T. Feld

Title: Associate Professor of Physics

Indicated at 2001, it was an attempt to determine if the defendant
was involved in the activities of the defendant and the defendant's

This report contains an account of the investigation conducted by the FBI in connection with the activities of the Communist Party, U.S.A., in the New York City area. The investigation was conducted by the New York City Office of the FBI, and the results are set forth in this report. The investigation was conducted in accordance with the provisions of the Espionage Laws, and the results are set forth in this report. The investigation was conducted in accordance with the provisions of the Espionage Laws, and the results are set forth in this report.

TABLE OF CONTENTS

	Page Number
I. INTRODUCTION	1
II. APPARATUS	6
DESCRIPTION OF SPECTROMETER	6
ELECTRONIC CIRCUIT	10
III. SELECTION OF PAIRS	19
IV. FUNCTION OF SCINTILLATOR NO. 3	23
V. RESOLUTION	24
LIGHT COLLECTION AND PHOTOMULTIPLIER STATISTICS	24
RADIATION ENERGY LOSS	25
ELECTRON ESCAPE	26
ENERGY LOSS IN THE CONVERTER	28
CAPTURE OF ANNIHILATION QUANTA	30
SUMMARY OF EXPECTED RESOLUTION	31
VI. CALIBRATION AT THE ROCKEFELLER ELECTROSTATIC GENERATOR	32
VII. DISCUSSION OF EXPERIMENTAL RESULTS	36
ENERGY CALIBRATION	36
FLUORINE RUNS	40
HIGH-ENERGY RUNS	45
VIII. SUMMARY	47
APPENDIX I. CALCULATION OF DIFFERENTIAL ENERGY LOSS DISTRIBUTION FOR SCINTILLATOR NO. 2 AT 17.6 Mev INCIDENT X-RAY ENERGY	48
Bibliography	51

STAYING TO STAY

Page Number

1 I. INTRODUCTION

2 II. APPARATUS

3

4

5

6

7

8

9

10

11

12

13

14

15

16

17

18

19

20

21

22

23

24

25

26

27

28

29

30

31

32

33

34

35

36

37

38

39

40

41

42

43

44

45

46

47

48

49

50

51

52

53

54

55

56

57

58

59

60

61

62

63

64

65

66

67

68

69

70

71

72

73

74

75

76

77

78

79

80

81

82

83

84

85

86

87

88

89

90

91

92

93

94

95

96

97

98

99

100

101

102

103

104

105

106

107

108

109

110

111

112

113

114

115

116

117

118

119

120

121

122

123

124

125

126

127

128

129

130

131

132

133

134

135

136

137

138

139

140

141

142

143

144

145

146

147

148

149

150

151

152

153

154

155

156

157

158

159

160

161

162

163

164

165

166

167

168

169

170

171

172

173

174

175

176

177

178

179

180

181

182

183

184

185

186

187

188

189

190

191

192

193

194

195

196

197

198

199

200

201

202

203

204

205

206

207

208

209

210

211

212

213

214

215

216

217

218

219

220

221

222

223

224

225

226

227

228

229

230

231

232

233

234

235

236

237

238

239

240

241

242

243

244

245

246

247

248

249

250

251

252

253

254

255

256

257

258

259

260

261

262

263

264

265

266

267

268

269

270

271

272

273

274

275

276

277

278

279

280

281

282

283

284

285

286

287

288

289

290

291

292

293

294

295

296

297

298

299

300

301

302

303

304

305

306

307

308

309

310

311

312

313

314

315

316

317

318

319

320

321

322

323

324

325

326

327

328

329

330

331

332

333

334

335

336

337

338

339

340

341

342

343

344

345

346

347

348

349

350

351

352

353

354

355

356

357

358

359

360

361

362

363

364

365

366

367

368

369

370

371

372

373

374

375

376

377

378

379

380

381

382

383

384

385

386

387

388

389

390

391

392

393

394

395

396

397

398

399

400

401

402

403

404

405

406

407

408

409

410

411

412

413

414

415

416

417

418

419

420

421

422

423

424

425

426

427

428

429

430

431

432

433

434

435

436

437

438

439

440

441

442

443

444

445

446

447

448

449

450

451

452

453

454

455

456

457

458

459

460

461

462

463

464

465

466

467

468

469

470

471

472

473

474

475

476

477

478

479

480

481

482

483

484

485

486

487

488

489

490

491

492

493

494

495

496

497

498

499

500

501

502

503

504

505

506

507

508

509

510

511

512

513

514

515

516

517

518

519

520

521

522

523

52

LIST OF ILLUSTRATIONS

	Page Number
Figure 1. Physical Arrangement of the Spectrometer	7
Figure 2. Arrangement and Shapes of the Plastic Scintillators	8
Figure 3. Construction of Scintillation Unit No. 1	9
Figure 4. Block Diagram of Experimental Equipment	12
Figure 5. Cable Curve	13
Figure 6. Block Diagram of the Addition and Gating Circuit	14
Figure 7. Block Diagram of the Pulse-Height Analysis Circuit	16
Figure 8. Method of Recording Scalar Lights	17
Figure 9. Calculated Differential Energy Distribution Curves for Scintillator No. 2, 17.6 Mev, 16-mil Pb Converter	20
Figure 10. Electron Energy Loss by Radiation	27
Figure 11. The Spectrometer in Place at the M.I.T. Rockefeller Generator	33
Figure 12. Calibration Curve	37
Figure 13. Energy Calibration	39
Figure 14. Pulse Height Distribution for Scintillator No. 2 at 6 Mev	41
Figure 15. Effect of Changing Discriminator No. 1	42
Figure 16. Effect of Changing Discriminator No. 2	44
Figure 17. Effect of the Anticoincidence Circuit at 17 Mev	46

1	Figure 1. General appearance of the locomotive
2	Figure 2. Arrangement and location of the wheels
3	Figure 3. Construction of the boiler
4	Figure 4. Plan of the boiler
5	Figure 5. Section of the boiler
6	Figure 6. Plan of the boiler
7	Figure 7. Section of the boiler
8	Figure 8. Plan of the boiler
9	Figure 9. Section of the boiler
10	Figure 10. Plan of the boiler
11	Figure 11. Section of the boiler
12	Figure 12. Plan of the boiler
13	Figure 13. Section of the boiler
14	Figure 14. Plan of the boiler
15	Figure 15. Section of the boiler
16	Figure 16. Plan of the boiler
17	Figure 17. Section of the boiler
18	Figure 18. Plan of the boiler
19	Figure 19. Section of the boiler
20	Figure 20. Plan of the boiler
21	Figure 21. Section of the boiler
22	Figure 22. Plan of the boiler
23	Figure 23. Section of the boiler
24	Figure 24. Plan of the boiler
25	Figure 25. Section of the boiler
26	Figure 26. Plan of the boiler
27	Figure 27. Section of the boiler
28	Figure 28. Plan of the boiler
29	Figure 29. Section of the boiler
30	Figure 30. Plan of the boiler
31	Figure 31. Section of the boiler
32	Figure 32. Plan of the boiler
33	Figure 33. Section of the boiler
34	Figure 34. Plan of the boiler
35	Figure 35. Section of the boiler
36	Figure 36. Plan of the boiler
37	Figure 37. Section of the boiler
38	Figure 38. Plan of the boiler
39	Figure 39. Section of the boiler
40	Figure 40. Plan of the boiler
41	Figure 41. Section of the boiler
42	Figure 42. Plan of the boiler
43	Figure 43. Section of the boiler
44	Figure 44. Plan of the boiler
45	Figure 45. Section of the boiler
46	Figure 46. Plan of the boiler
47	Figure 47. Section of the boiler
48	Figure 48. Plan of the boiler
49	Figure 49. Section of the boiler
50	Figure 50. Plan of the boiler
51	Figure 51. Section of the boiler
52	Figure 52. Plan of the boiler
53	Figure 53. Section of the boiler
54	Figure 54. Plan of the boiler
55	Figure 55. Section of the boiler
56	Figure 56. Plan of the boiler
57	Figure 57. Section of the boiler
58	Figure 58. Plan of the boiler
59	Figure 59. Section of the boiler
60	Figure 60. Plan of the boiler
61	Figure 61. Section of the boiler
62	Figure 62. Plan of the boiler
63	Figure 63. Section of the boiler
64	Figure 64. Plan of the boiler
65	Figure 65. Section of the boiler
66	Figure 66. Plan of the boiler
67	Figure 67. Section of the boiler
68	Figure 68. Plan of the boiler
69	Figure 69. Section of the boiler
70	Figure 70. Plan of the boiler
71	Figure 71. Section of the boiler
72	Figure 72. Plan of the boiler
73	Figure 73. Section of the boiler
74	Figure 74. Plan of the boiler
75	Figure 75. Section of the boiler
76	Figure 76. Plan of the boiler
77	Figure 77. Section of the boiler
78	Figure 78. Plan of the boiler
79	Figure 79. Section of the boiler
80	Figure 80. Plan of the boiler
81	Figure 81. Section of the boiler
82	Figure 82. Plan of the boiler
83	Figure 83. Section of the boiler
84	Figure 84. Plan of the boiler
85	Figure 85. Section of the boiler
86	Figure 86. Plan of the boiler
87	Figure 87. Section of the boiler
88	Figure 88. Plan of the boiler
89	Figure 89. Section of the boiler
90	Figure 90. Plan of the boiler
91	Figure 91. Section of the boiler
92	Figure 92. Plan of the boiler
93	Figure 93. Section of the boiler
94	Figure 94. Plan of the boiler
95	Figure 95. Section of the boiler
96	Figure 96. Plan of the boiler
97	Figure 97. Section of the boiler
98	Figure 98. Plan of the boiler
99	Figure 99. Section of the boiler
100	Figure 100. Plan of the boiler

ACKNOWLEDGMENTS

The author* expresses his appreciation to all those who have helped to make this work possible. He is particularly indebted to Dr. P. T. Demos for friendly guidance and helpful advice throughout the course of this and other work; to Dr. C. P. Sargent for active participation in all phases of the experimental work; to Professor R. D. Evans and Professor B. T. Feld for advice in various phases of the experiment and theory; to Dr. Hans Mark for making the facilities of the Rockefeller generator available and for many other kindnesses and helpful suggestions; to Mr. H. W. Greene for help in the construction of the electronic components.

For the typing and proofreading, the author would like to express his special thanks to Mrs. Mary E. White. Thanks are also due Mrs. Grace Rowe for making the drawings and to Mr. N. Saia for making the block diagrams.

* Enrolled at the Massachusetts Institute of Technology under the United States Naval Postgraduate School system through the sponsorship of the Bureau of Ordnance, Navy Department.

ACKNOWLEDGMENTS

The author expresses his appreciation to all those who have helped him in this work. He is particularly indebted to Dr. F. J. Owens for his helpful criticism and advice throughout the course of this and other work; to Dr. C. R. Sargent for his criticism in all phases of the experimental work; to Professor A. H. Swann and Professor B. T. Fildes for their interest in the progress of the work; to Dr. J. H. Dyer for making the facilities of the Rockefeller Institute available and for many other kindnesses and helpful suggestions; to Dr. F. J. Owens for help in the construction of the electric circuits.

For the typing and proofreading, the author would like to express his special thanks to Mrs. Mary E. White. Thanks are also due Mrs. Dyer for making the drawings and to Mr. H. J. Dyer for making the plate diagrams.

Published at the Rockefeller Institute of Technology under the title of the Rockefeller Research Series through the generosity of the Howard at Graduate, New York Department.

I. INTRODUCTION

The intention of this paper is to describe an x-ray spectrometer designed for use at the M. I. T. linear accelerator. The spectrometer is a three-counter telescope with a thin lead radiator between the first and second counter. The first and second counters are thin plastic scintillators; the third, a thick plastic scintillator. An acceptable event is one in which there is no pulse in the first counter and a doubly ionizing pulse in the second counter in coincidence with the third counter. Such events should be electron-positron pairs originating only in the radiator. To a first approximation, the sum of the pulse heights produced in the second and third counter is proportional to the incident x-ray energy. This chapter is devoted to explaining the need for a spectrometer of this type at the linear accelerator.

Five- to 25-Mev x-rays are known to interact strongly with nuclei. Among the heavier elements, as much as 2 percent of the total absorption coefficient for 25-Mev bremsstrahlung is of nuclear rather than atomic origin. Most of the experiments have investigated the emission of heavy particles following photon absorption. Recently, however, some measurements have been made of nuclear absorption coefficients in good geometry transmission experiments¹ and of large-angle scattering of bremsstrahlung².

1. INTRODUCTION

The invention of this paper is to describe an x-ray spectrometer designed for use at the M.I.T. Linear Accelerator. The spectrometer is a three-counter telescope with a thin lead collimator between the first and second counters. The first and second counters are thin plastic scintillators; the third, a thin plastic scintillator. An acceptable event is one in which there is no pulse in the first counter and a doubly ionizing pulse in the second counter in coincidence with the third counter. Such events should be electron-positron pairs originating only in the collimator. To a first approximation, the sum of the pulse heights produced in the second and third counter is proportional to the incident x-ray energy. This chapter is devoted to describing the need for a spectrometer of this type at the linear accelerator.

The 100-GeV x-rays are known to interact strongly with nuclei. From the earlier experiments, as much as 5 percent of the total absorption coefficient for 100-GeV bremsstrahlung is of nuclear rather than atomic origin. Most of the experiments have investigated the relation of heavy nuclei to the total absorption. Recently, however, some experiments have been made of nuclear absorption coefficients in lead counter telescope experiments and of their contribution to the total absorption.

The M. I. T. linear accelerator is 10 to 100 times as strong a source of 5- to 17-Mev x-rays as the usual betatron of comparable energy. This accelerator can furnish average electron currents of about 2 microamperes. It is, however, a pulsed machine with a duty ratio of only 10^{-4} , and during the 1 microsecond pulse, the current reaches peaks of about 50 milliamperes. The low-duty ratio of the accelerator is a very important factor in the design of an x-ray spectrometer for use at the M.I.T. linear accelerator. The counting rate of a detector can be no more than a few counts per second, and the detector must be able to operate in the presence of a very high level of background radiation (low-energy photons and fast neutrons) present during the 1 microsecond pulse. One must use this high photon intensity of the accelerator to obtain energy resolution, good geometry, or small target size, rather than to obtain high counting rates.

A second limitation of the M. I. T. linear accelerator as a photon source imposes further restrictions on a photon detector. The electron energy spectrum of the accelerator is not only far from monochromatic, but it is difficult to keep the spectrum constant during a run and difficult to reproduce the same spectrum on subsequent runs. If one is to use all the current available and, say, thick-target bremsstrahlung in order to make as strong a photon source as possible, it is:

1. Necessary to monitor the photon spectrum itself rather than the electron current; and

The M. I. T. linear accelerator is 10 to 100 times as strong a

source of 5- to 15-Mev rays as the small detector of comparable energy. This accelerator can furnish average electron currents of about 5 microamperes. It is, however, a pulsed machine with a duty ratio of only 10^{-4} , and during the 1 microsecond pulse, the current reaches a peak of about 50 milliamperes. The low-duty ratio of the accelerator is a very important factor in the design of an x-ray spectrometer for use at the M. I. T. linear accelerator. The operating rate of a detector can be no more than a few counts per second, and the detector must be able to operate in the presence of a very high level of background radiation (low-energy photons and fast neutrons) without being overloaded. One must use this high degree of selectivity of the accelerator to obtain energy resolution, good energy, or small energy size, rather than to obtain high counting rates.

A second limitation of the M. I. T. linear accelerator as a photon source comes from the fact that the detector is not only for the electron energy spectrum of the accelerator but is also for the electron energy spectrum. It is difficult to keep the electron current down to a few and sufficient to reproduce the same spectrum as independent runs. It can be seen that the current available may, say, change by a factor of 10 in order to obtain a photon source as

possible, it is

1. Because of the fact that the photon spectrum itself

varies with the electron current, and

2. Very desirable to obtain as much information as possible from a single run.

The most efficient photon detector with reasonable resolution is a large volume of NaI. Such a spectrometer has been constructed by Koch³. Koch's best detector is a total absorption spectrometer with 11 percent resolution at 11 Mev, employing a NaI crystal 5 x 8 inches. His 2 x 2 x 5-inch NaI crystal gives about 20 percent resolution at 10 Mev. For use at the accelerator, the expense of such a large amount of NaI would perhaps be justified were it not for

1. The extreme sensitivity of NaI to photon radiation;
2. Its relative slow decay time of about 0.3 μ sec.

The first limitation requires the spectrometer to be enclosed in a massive amount of shielding. In a large-angle photon scattering experiment, the signal would need to be clipped to a fraction of the decay time of NaI to reduce pile-up of Compton recoil electrons. The differential cross section for Compton scattering at 90 degrees is as much as 10^5 times as large as cross sections one would like to measure, and the pile-up of the approximately half Mev Compton scattered photons during the 1 μ second accelerator pulse is a serious problem with any photon detector which involves pulse-height analysis.

The best energy resolution in the 5- to 17-Mev region is obtained with a magnetic pair spectrometer. Walker and McDaniel⁴ were among the first in this field and obtained a solid angle times efficiency of approximately 10^{-7} with an energy resolution (width at half

maximum) of 5.5 percent. Currently, the best energy resolution in the 5- to 17-Mev energy range is obtained by Kinsey and Bartholomew⁵, using a similar improved version of Walker and McDaniel's magnetic pair spectrometer. Using a 4.7 milligram/cm² gold radiator, Kinsey's best half-width is 140 kev, independent of photon energy.

The linear accelerator is a sufficiently strong source of x-rays to enable one to utilize a high-resolution, low-efficiency magnetic pair spectrometer. It should be able to measure the entire energy spectrum at one time; hence, it would have many channels and be of large size.

Another type of spectrometer, known as the three-crystal scintillation spectrometer⁶⁻⁸, employing three NaI 1-1/2 inch diameter crystals proves useful in the 4- to 12-Mev energy range. A typical arrangement⁶ employs two 1-1/2 inch by 1 inch thick NaI crystals as annihilation radiation detectors and a center 1-1/2 inch by 4 inch long NaI crystal which measures the energy of the coincidence pair. Counter efficiency at 6 Mev is about 10^{-5} , and width at half maximum is 7 percent.

Energy resolution with this three-crystal scintillation spectrometer at 11 Mev is 11 percent. In addition to these limitations imposed by the linear accelerator on the NaI total absorption spectrometer, the three-crystal scintillation spectrometer depends on 0.51-Mev photons in coincidence for its resolution, and hence is not easily adaptable for use at the M.I.T. linear accelerator.

maximum) of 2.5 percent. Currently, the best energy resolution in the 7- to 15-Mev energy range is obtained by Kinsey and Rutherford's using a shielded improved version of Wilson and Rutherford's magnetic pair spectrometer. Using a 0.7 millimeter gold radiator, Kinsey's best half-width is 150 keV, independent of photon energy.

The linear accelerator is a sufficiently strong source of x-rays to enable one to utilize a high-resolution, low-efficiency magnetic pair spectrometer. It should be able to measure the entire energy spectrum at one time; hence, it would have many channels and be of large size.

Another type of spectrometer, known as the three-crystal coincidence spectrometer, employing three 1-1/2 inch thick crystals proves useful in the 4- to 15-Mev energy range. A typical arrangement employs two 1-1/2 inch by 1 inch thick NaI crystals as anti-scatter radiation detectors and a center 1-1/2 inch by 1 inch NaI crystal which measures the energy of the coincident pair. Counter efficiency at 6 Mev is about 10%, and width at half maximum is 7 percent.

Energy resolution with this three-crystal coincidence spectrometer at 11 Mev is 11 percent. In addition to these limitations imposed by the linear accelerator on the full absorption spectrometer, the three-crystal coincidence spectrometer depends on 0.51-Mev photons in coincidence for its resolution, and hence is not easily adaptable for use at the A.T.T. linear accelerator.

A fourth approach to the problem has been attempted, which should provide:

1. Approximately 10 percent resolution at 10 Mev;
2. Small dimensions and ease of shielding;
3. Solid-angle times efficiency of about 10^{-4} ;
4. Ability to measure an entire spectrum of photons from 5- to 17-Mev at a single run with several bins per resolution width;

5. Simplicity and economy as far as the actual detection is concerned. The major investment would go into the design and construction of associated electronic equipment. This same equipment would be useful for other projects at the M. I. T. accelerator (see, for example, W. J. Sawtelle, S.M. Thesis, M.I.T., May 1955).

A fourth aspect of the problem has been suggested, which

should provide:

1. Approximately 10 percent resolution at 10 days;

2. Half resolution and cost of shipping;

3. Half-time efficiency of about 10%;

4. Ability to measure an entire spectrum of phenomena

from 2-20 eV at a single run with several days per resolution

width.

5. Simplicity and economy as far as the actual data-

tion is concerned. The major investment would go into the design and

construction of associated electronic equipment. This same equipment

would be useful for other projects of the U.S. Accelerator (see,

for example, W. J. Stroh, W. K. Treadwell, W. I. T. Rep. 1957).

6. The design of the instrument should be such that it can be

used for a wide range of experiments with a minimum of

modification of the instrument.

7. The instrument should be able to operate at 10 eV and

at 20 eV.

8. The instrument should be able to operate at 10 eV and

at 20 eV.

9. The instrument should be able to operate at 10 eV and

at 20 eV.

10. The instrument should be able to operate at 10 eV and

at 20 eV.

11. The instrument should be able to operate at 10 eV and

II. APPARATUS

DESCRIPTION OF SPECTROMETER

The spectrometer scintillators are commercially available "Pilot B" crystals, density 1.03, polyvinyl toluene, para-terphenyl, para-para-prime diphenylstilbene¹⁹. Preliminary measurements indicate a decay time of less than 3×10^{-9} seconds²⁰. Figure 1 shows to scale the physical arrangement of the spectrometer. The beam of photons from the source being surveyed is collimated by means of a half-inch hole in a 3-inch thick lead disk. The collimated photons are then incident on a lead foil where they interact forming pairs and Compton recoil electrons. This foil is known as the "converter." The converter is one-half inch in diameter, cemented to a thin lucite ring. The converter fits flush against scintillator No. 2, which in turn is held flush against scintillator No. 1. No. 2 scintillator is a cylinder $3/4$ inch in diameter by $3/16$ inch thick; No. 1 scintillator is a tapered cylinder 3 inches long, tapering from $2-1/4$ inches in diameter to $1-1/2$ inches in diameter one-half inch from the end. Figure 2 shows the shape and arrangement of the plastic scintillators.

Scintillator No. 1 has all its open faces wrapped in 1-mil aluminum foil to improve the light collection and to separate optically scintillator No. 1 from scintillator No. 2. The scintillation unit comprises the plastic scintillator, optical coupling, and selected RCA 5819 phototube. Figure 3 shows to scale the method of construction of unit No. 1.

EXPERIMENTAL RESULTS

The experimental results are summarized in the following table.

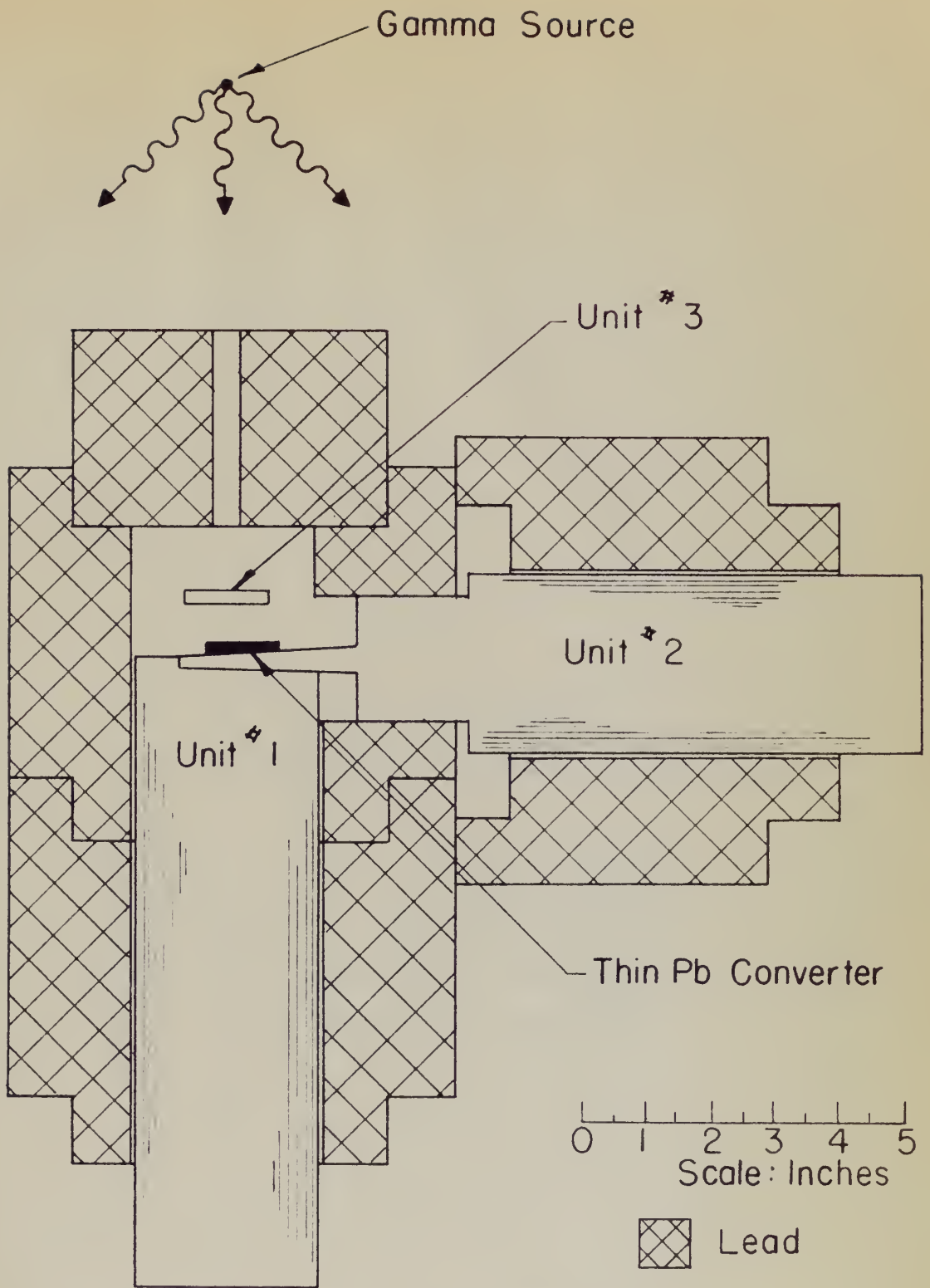
1. The experimental results are summarized in the following table.	2. The experimental results are summarized in the following table.	3. The experimental results are summarized in the following table.	4. The experimental results are summarized in the following table.	5. The experimental results are summarized in the following table.	6. The experimental results are summarized in the following table.	7. The experimental results are summarized in the following table.	8. The experimental results are summarized in the following table.	9. The experimental results are summarized in the following table.	10. The experimental results are summarized in the following table.	11. The experimental results are summarized in the following table.	12. The experimental results are summarized in the following table.	13. The experimental results are summarized in the following table.	14. The experimental results are summarized in the following table.	15. The experimental results are summarized in the following table.	16. The experimental results are summarized in the following table.	17. The experimental results are summarized in the following table.	18. The experimental results are summarized in the following table.	19. The experimental results are summarized in the following table.	20. The experimental results are summarized in the following table.
--	--	--	--	--	--	--	--	--	---	---	---	---	---	---	---	---	---	---	---

Figure 1

Physical Arrangement of the Spectrometer

The axis of scintillator unit No. 3 is perpendicular to both the axis of unit No. 2 and unit No. 1.

Figure 1



SHIELDING ARRANGEMENT

Figure 2

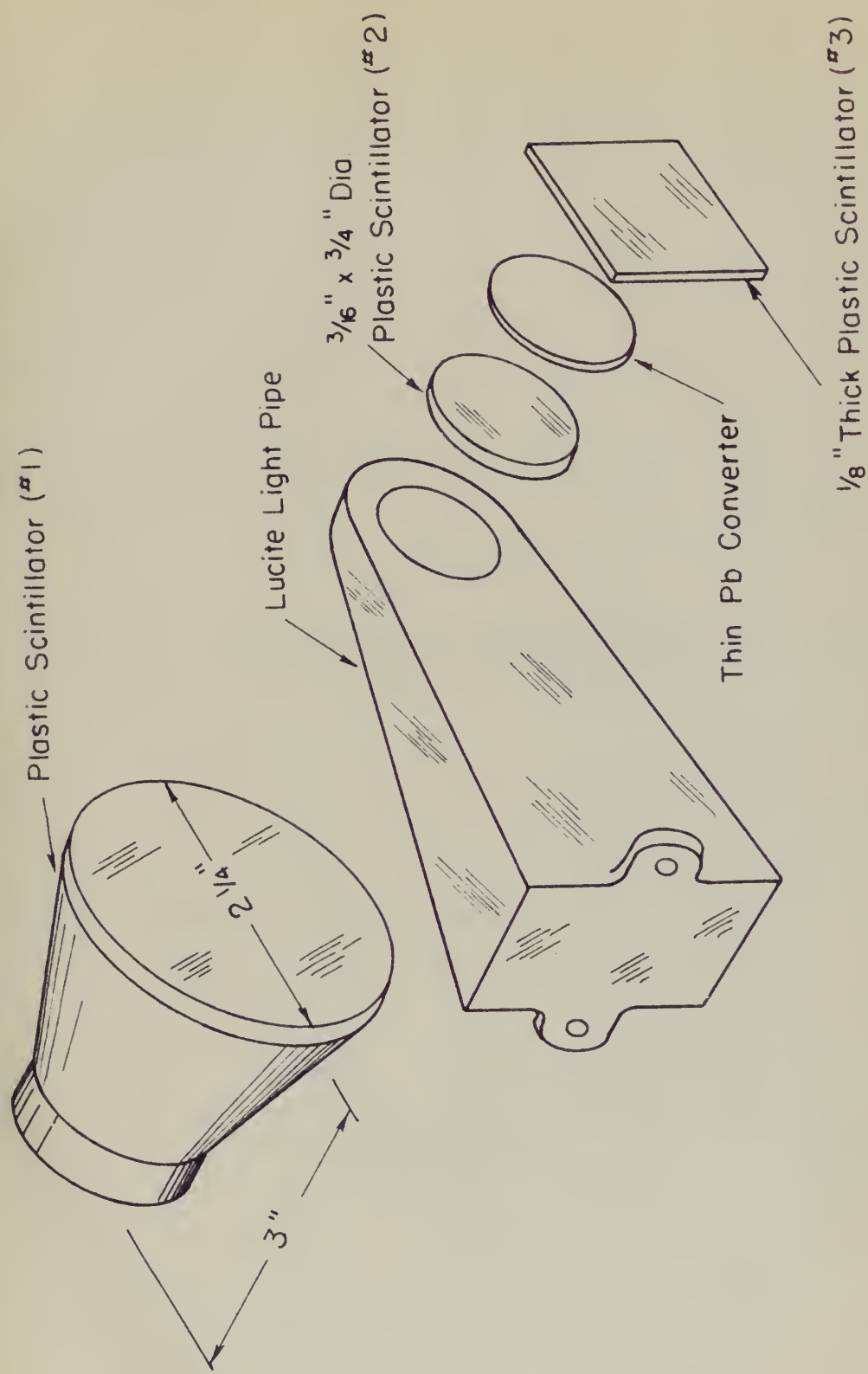
Arrangement and Number of the
Plastic Reinforcers

Plastic reinforcer No. 2 is a push fit into
the inside light pipe. The connector, No. 3
reinforcer, and reinforcer No. 1 are held
together by a clamp arrangement.

Figure 2

Arrangement and Shapes of the
Plastic Scintillators

Plastic scintillator No. 2 is a push fit into the lucite light pipe. The converter, No. 2 scintillator, and scintillator No. 1 are held together by a clamp arrangement.



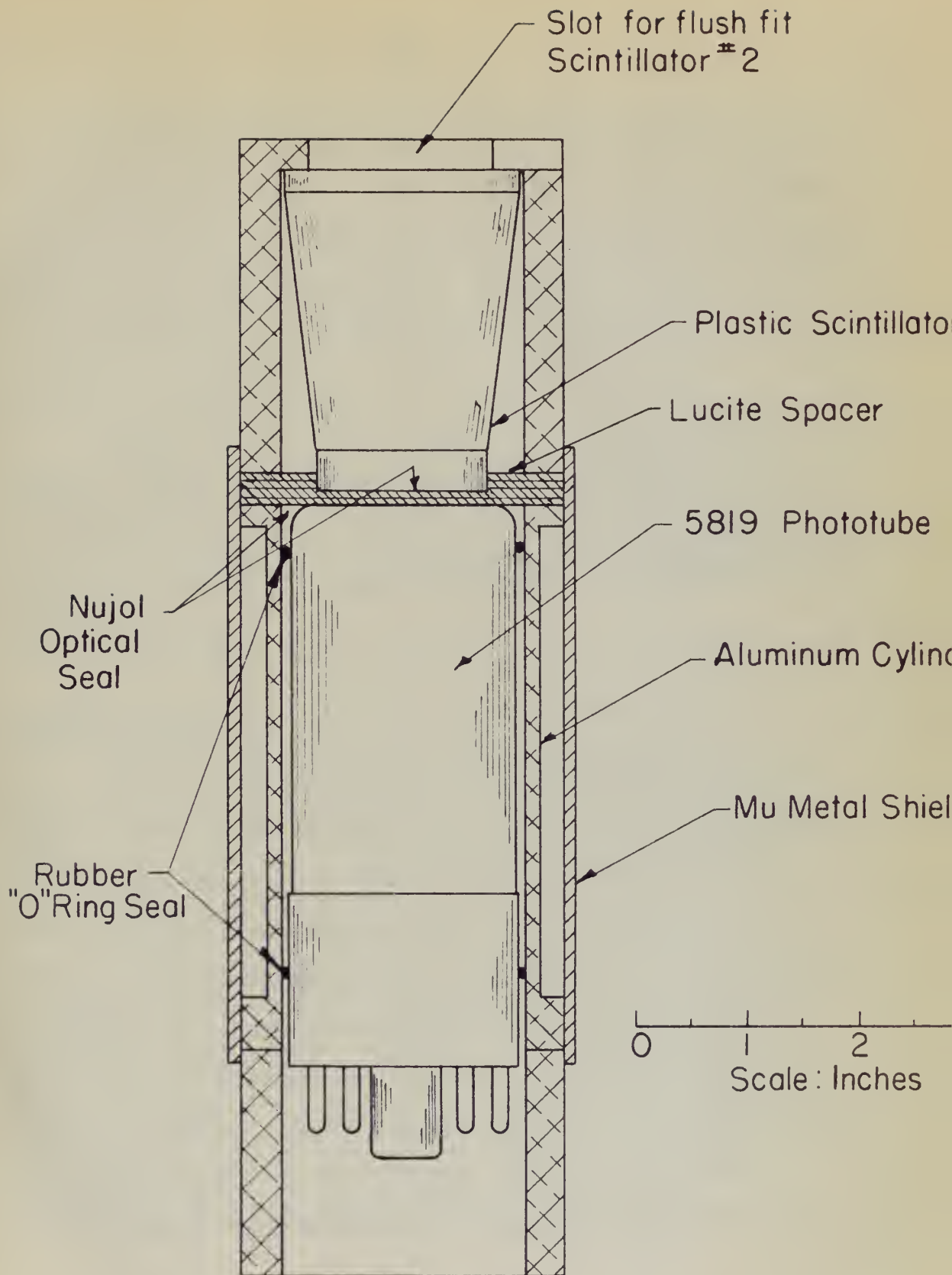
ARRANGEMENT OF PLASTIC SCINTILLATORS

Figure 3

Construction of Scintillation Unit No. 1.

Figure 3

Comparison of behavior of the system



SCINTILLATION UNIT #1

Scintillator unit No. 2 has a 1-1/2 inch diameter, 2 inch long lucite light pipe, to which is screwed the 2-1/2 inch lucite light pipe shown in Figure 2. Scintillator No. 2 is inserted in the light pipe (push fit, Mujol optical seal). The converter holder fits into a larger diameter, 1/4 inch thick lucite ring which clamps unit No. 1 and unit No. 2 together.

Scintillator No. 3 is 1/8 inch by 1-1/8 inch, rectangular cross section, 2 inches long (shown in Figure 2). This domino-shaped plastic scintillator is held by a lucite clamp so that the standard 1-1/2 inch diameter lucite light pipe (as described for scintillator No. 2) looks at it end on.

ELECTRONIC CIRCUIT

The experimental equipment is shown in the block diagram of Figure 4. The gain of the system is calibrated by introducing artificial pulses (employing a Western Electric 275B relay to develop pulses of proper shape) into the input of the preamplifier. The height of these pulses is measured to an accuracy of a few tenths of a percent. The preamplifier is physically located as an integral part of the scintillation unit, bolted to the end of the aluminum housing of Figure 3. Pulses are then amplified times 30 in an amplifier whose rise time is 0.04 μ second. Unit No. 1 and unit No. 2 have two outputs. One output goes to the coincidence circuit and

Sensitizer unit No. 2 has a 1-1/2 inch diameter, 2 inch long
inside light pipe, to which is screwed the 2-1/2 inch inside light
pipe shown in Figure 2. Sensitizer No. 2 is inserted in the light
pipe (with its optical seal). The converter holder fits into
a larger diameter, 1/2 inch thick inside ring which clamps unit No. 1
and unit No. 2 together.

Sensitizer No. 3 is 1 1/4 inch by 1-1/2 inch, rectangular cross
section, 2 inches long (shown in Figure 3). This dome-shaped plas-
tic sensitizer is held by a inside clamp so that the standard 1-1/2
inch diameter inside light pipe (as described for sensitizer No. 2)
locks at its end.

EXPERIMENTAL CIRCUIT

The experimental arrangement is shown in the block diagram of
Figure 4. The input of the system is calibrated by introducing arti-
ficial pulses (using a Western Electric 25M relay to develop
pulses of known shape) into the input of the photomultiplier. The
height of these pulses is measured to an accuracy of a few tenths of
a percent. The photomultiplier is typically located at an interval
part of the excitation wave, placed at the end of the aluminum
housing as shown in Figure 5. Pulses are then amplified three to an ampli-
fier whose gain is 0.01 to 10. Unit No. 1 and unit No. 2
have two outputs. The output goes to the coincidence circuit and

the other to the addition circuit. The coincidence outputs from unit No. 1 and unit No. 2 are delay-line clipped to 0.05μ second and delayed by 0.03μ second to allow time for anticoincidence pulse No. 3 to function. These pulses are amplified and fed into an EFP 60-pulse shaper. The function of D2 is to discriminate against the Compton recoil electrons. D1 allows the biasing out of low-energy photons if desired. The output of EFP 60 No. 3 goes to the grid of the No. 2 Philips tube. Since the two inputs of the No. 2 EFP 60 are out of phase, if a signal exists at No. 3, there is no output from No. 2. The outputs of the No. 1 and No. 2 pulse shapers go to a diode bridge.

The measurement of the resolving time of the spectrometer was experimentally determined, using the 6-Mev fluorine gamma-ray, to be 0.057μ second, as shown in Figure 5. A DuMont 6292 phototube was tried in unit No. 1 but proved to be unsatisfactory. The fluctuations in the transit time for the DuMont tube were so large that the cable curve was not flat on top.

The other outputs from the No. 1 and No. 2 (x 30) amplifiers are added, clipped to 0.08μ second, stretched, and amplified as shown by the block diagram of Figure 6. The output from the diode-bridge coincidence circuit triggers a univibrator which forms a 10μ second gate. If the gate is open, the added pulse gets through and is amplified and then is pulse height analyzed.

[illegible]

The movement of the resolving film of the spectrometer was approximately determined, using the 5-day fluorine gamma-ray, to be 0.037 a second, as shown in Figure 2. A second 5-day fluorine gamma-ray was used to check this. I had proved to be unnecessary. The fluorine gamma-ray in the spectrum for the 5-day fluorine was so large that the

The other outputs from the No. 1 and No. 2 amplifiers are added, summed, and amplified as shown by the block diagram of Figure 4. The output from the discriminator is also added to the sum of the two other outputs and is amplified and summed as shown by the block diagram of Figure 5. The output from the discriminator is also added to the sum of the two other outputs and is amplified and summed as shown by the block diagram of Figure 5.

Figure 4

Block Diagram of Experimental Equipment

The addition and gating circuit is shown in Figure 6, the pulse-height analysis circuit in Figure 7.

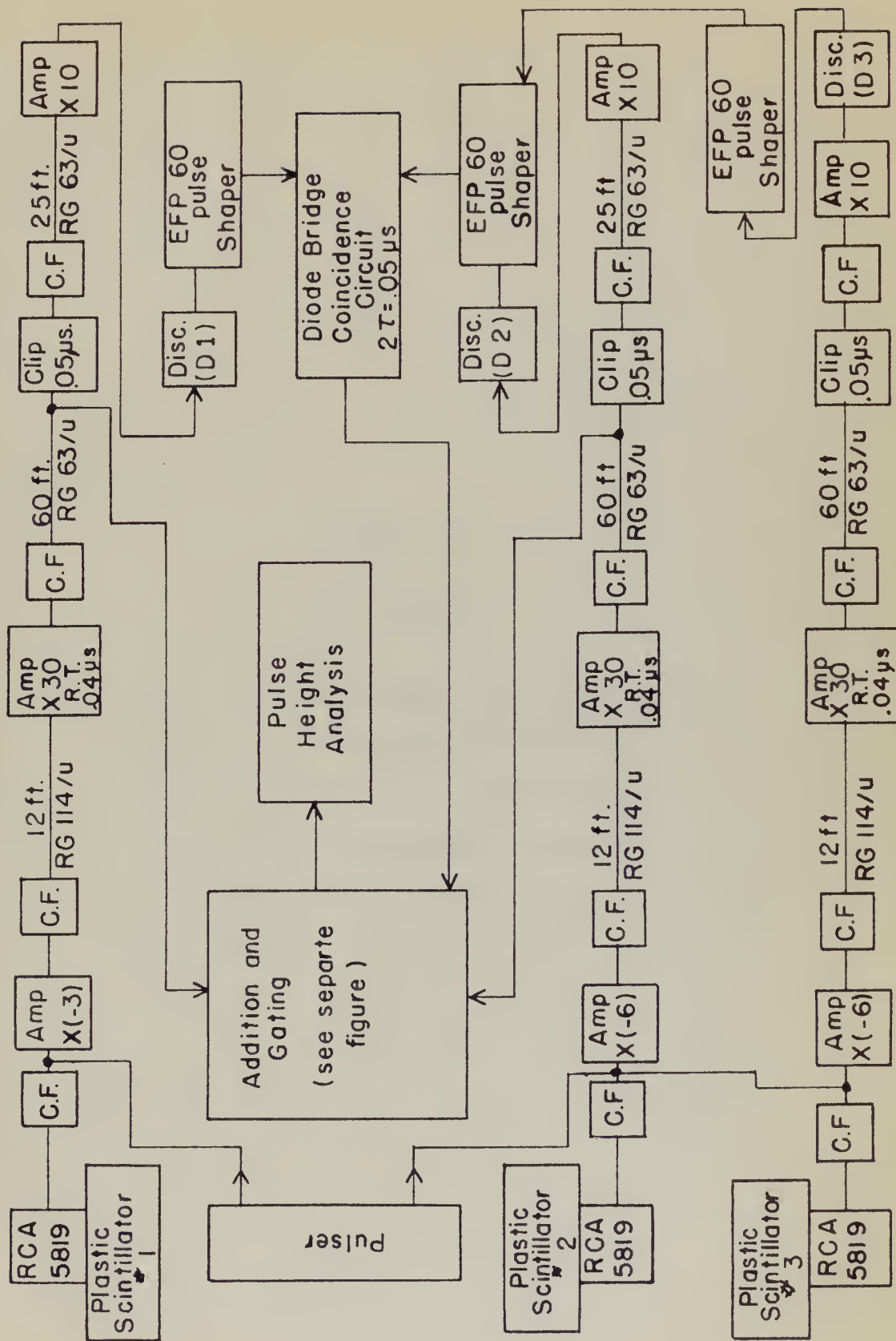
Page 2

THE HISTORY OF THE UNITED STATES

The history and development of the United States

from the first settlement to the present day

in 1776



DI CCK DIA CDA M CE EXPEDIMENTAL EOLUDMENT

Figure 5

Cable Curve

RG 63/U was used in conjunction with a $F^{19}(p, \alpha' \gamma)$ source to determine experimentally the resolving time of the spectrometer. Each run was normalized to the same number of protons incident on the proton target.

Figure 2

Table 1

At 60 V was used in connection with a
100 (2, 2) source to determine experimen-
tally the resolving time of the spec-
trum. Each run was normalized to the
same number of protons incident on the
proton target.

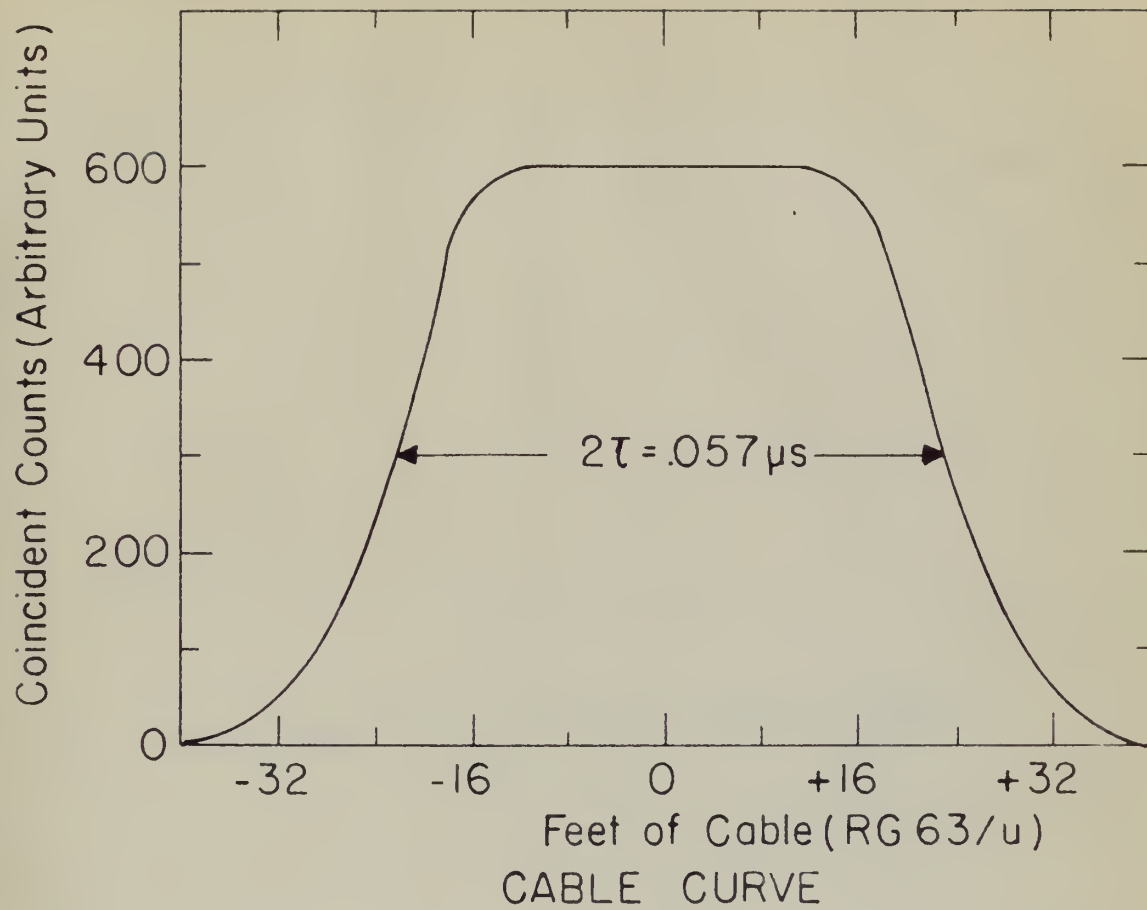
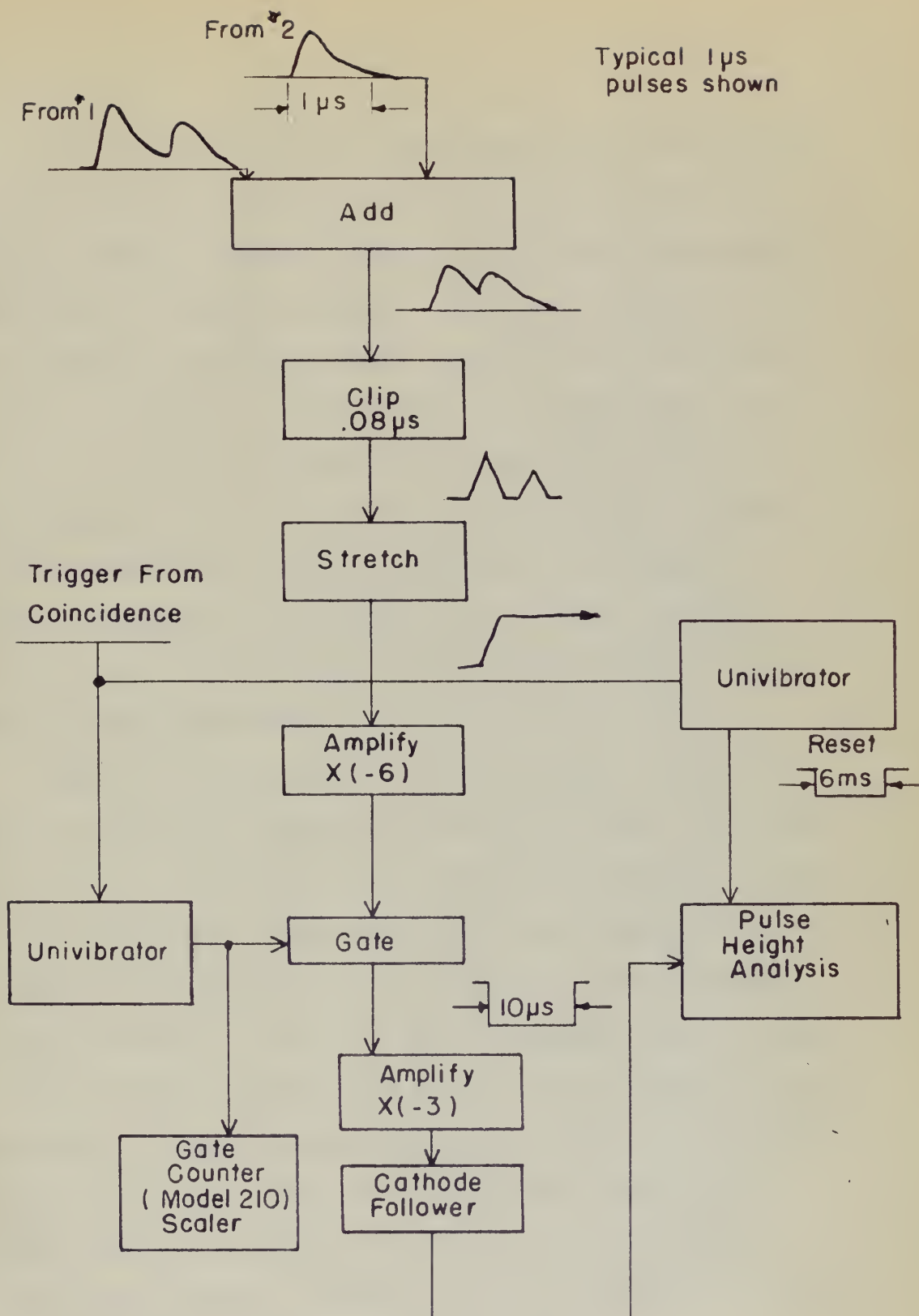


Figure 6

Block Diagram of the Addition and Gating Circuit.

Figure 6

Black squares of the addition and subtraction



ADDITION AND GATING CIRCUIT

The pulse-height analysis circuit-block diagram is given in Figure 7. The basic principle of this pulse-height analysis is that pulse height is changed to time by a condenser discharging at constant current through a pentode. This time is accurately measured by beating a crystal-controlled oscillator on the triangular pulse and counting the oscillator pulses by a conventional binary scaler. This circuit is known as the "Multichannel Differential Discriminator," and its detailed circuit diagram may be found on file 6432, Laboratory for Nuclear Science, M. I. T., Dwg. No. D-2231-A. The output of the scaler goes to a buffer amplifier and then to one of two (or both simultaneously) methods of recording the reading of the scaler.

Figure 8 shows one method of data recording. This method provides a 128-channel recording pulse-height analyzer. Six scaler lights are in a light-tight box where they are recorded by a standard 16-mm movie camera externally driven at approximately 9 inches per minute. The framing pawl of the camera is removed to achieve continuous movement of the film. This is necessary, since the film is "framed" even though the camera shutter has been removed and made inoperative. A clock is an added feature for future identification. The film is read most easily by scanning it on a standard 16-mm microfilm reader. The pulser is turned on periodically during a run for calibration purposes. Reading time varies from 150 - 400 counts per hour, depending on energy and counting rate.

The pulse-height analysis circuit-block diagram is given in

Figure 7. The basic principle of this pulse-height analysis is that pulse height is changed to time by a condenser discharging at constant current through a period. This time is accurately measured by feeding a crystal-controlled oscillator on the triangular pulse and counting the oscillator pulses by a conventional binary scaler. This circuit is known as the "Weinmann Differential Discriminator," and the detailed circuit diagram may be found on file 612, Laboratory for Nuclear Science, M. I. T., Eng. No. D-2311-4. The output of the scaler goes to a buffer amplifier and then to one of two (or both simultaneously) methods of recording the reading of the scaler.

Figure 8 shows one method of data recording. This method provides a 157-channel recording pulse-height analyzer. Six scaler lights are in a light-tight box where they are recorded by a standard 16-mm movie camera externally driven at approximately 9 inches per minute. The framing panel of the camera is removed to achieve continuous movement of the film. This is necessary, since the film is "frozen" even though the camera shutter has been removed and made insensitive. A clock is an added feature for future identification. The film is read most easily by scanning it on a standard 16-mm microfilm reader. The viewer is turned on periodically during a run for calibration purposes. Reading time varies from 150 - 100 counts per hour, depending on energy and counting rate.

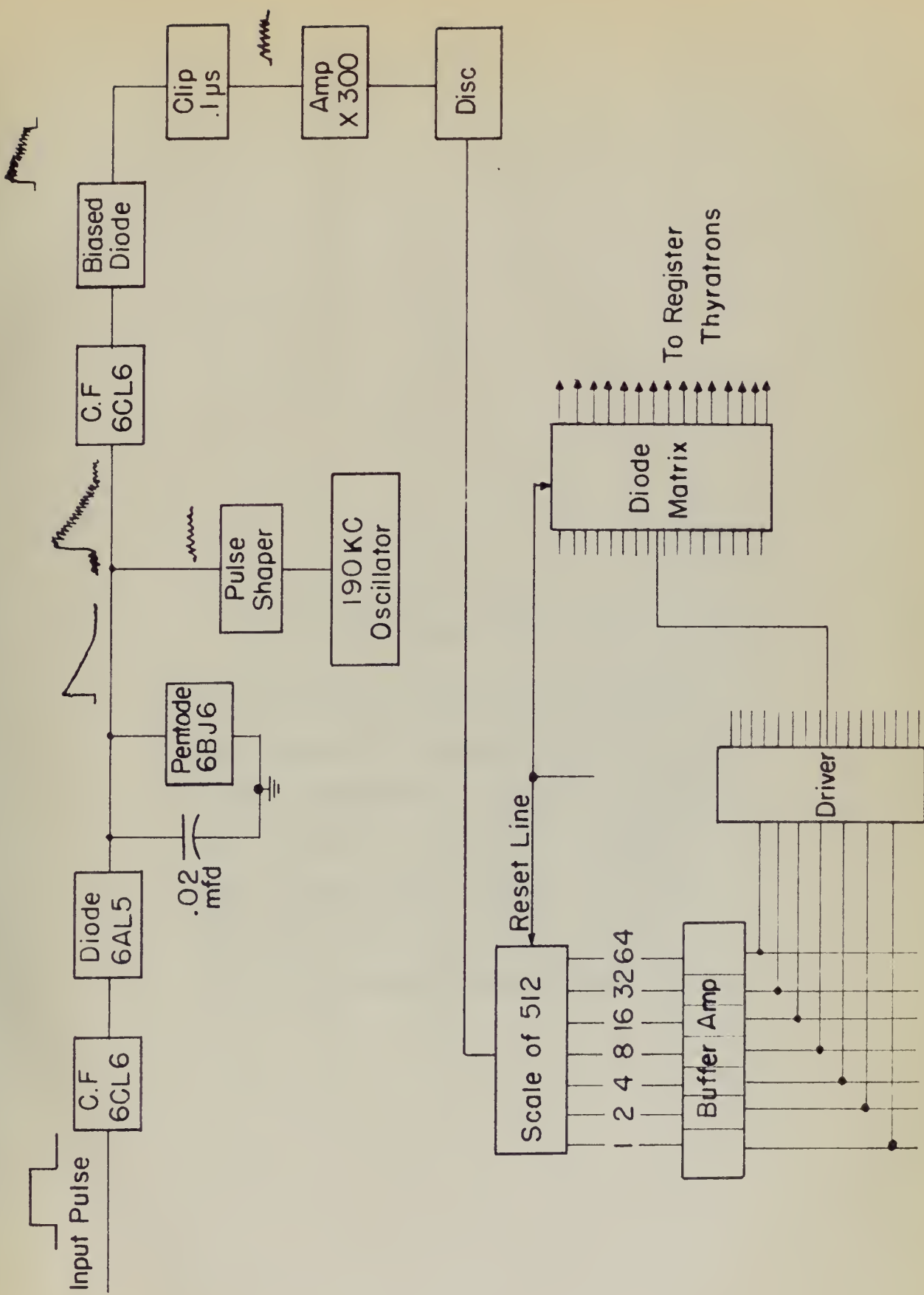
Figure 7

Block Diagram of the Pulse-Height Analysis Circuit

The following is a summary of the results of the study. The first part of the study was a survey of the general public. The results of this survey are shown in Table I. The second part of the study was a survey of the medical profession. The results of this survey are shown in Table II. The third part of the study was a survey of the legal profession. The results of this survey are shown in Table III. The fourth part of the study was a survey of the business community. The results of this survey are shown in Table IV. The fifth part of the study was a survey of the academic community. The results of this survey are shown in Table V. The sixth part of the study was a survey of the religious community. The results of this survey are shown in Table VI. The seventh part of the study was a survey of the entertainment community. The results of this survey are shown in Table VII. The eighth part of the study was a survey of the government community. The results of this survey are shown in Table VIII. The ninth part of the study was a survey of the military community. The results of this survey are shown in Table IX. The tenth part of the study was a survey of the scientific community. The results of this survey are shown in Table X.

Black Studies of the Black-White Issue

The following is a summary of the results of the study. The first part of the study was a survey of the general public. The results of this survey are shown in Table I. The second part of the study was a survey of the medical profession. The results of this survey are shown in Table II. The third part of the study was a survey of the legal profession. The results of this survey are shown in Table III. The fourth part of the study was a survey of the business community. The results of this survey are shown in Table IV. The fifth part of the study was a survey of the academic community. The results of this survey are shown in Table V. The sixth part of the study was a survey of the religious community. The results of this survey are shown in Table VI. The seventh part of the study was a survey of the entertainment community. The results of this survey are shown in Table VII. The eighth part of the study was a survey of the government community. The results of this survey are shown in Table VIII. The ninth part of the study was a survey of the military community. The results of this survey are shown in Table IX. The tenth part of the study was a survey of the scientific community. The results of this survey are shown in Table X.



PULSE HEIGHT ANALYSIS CIRCUIT

Figure 8

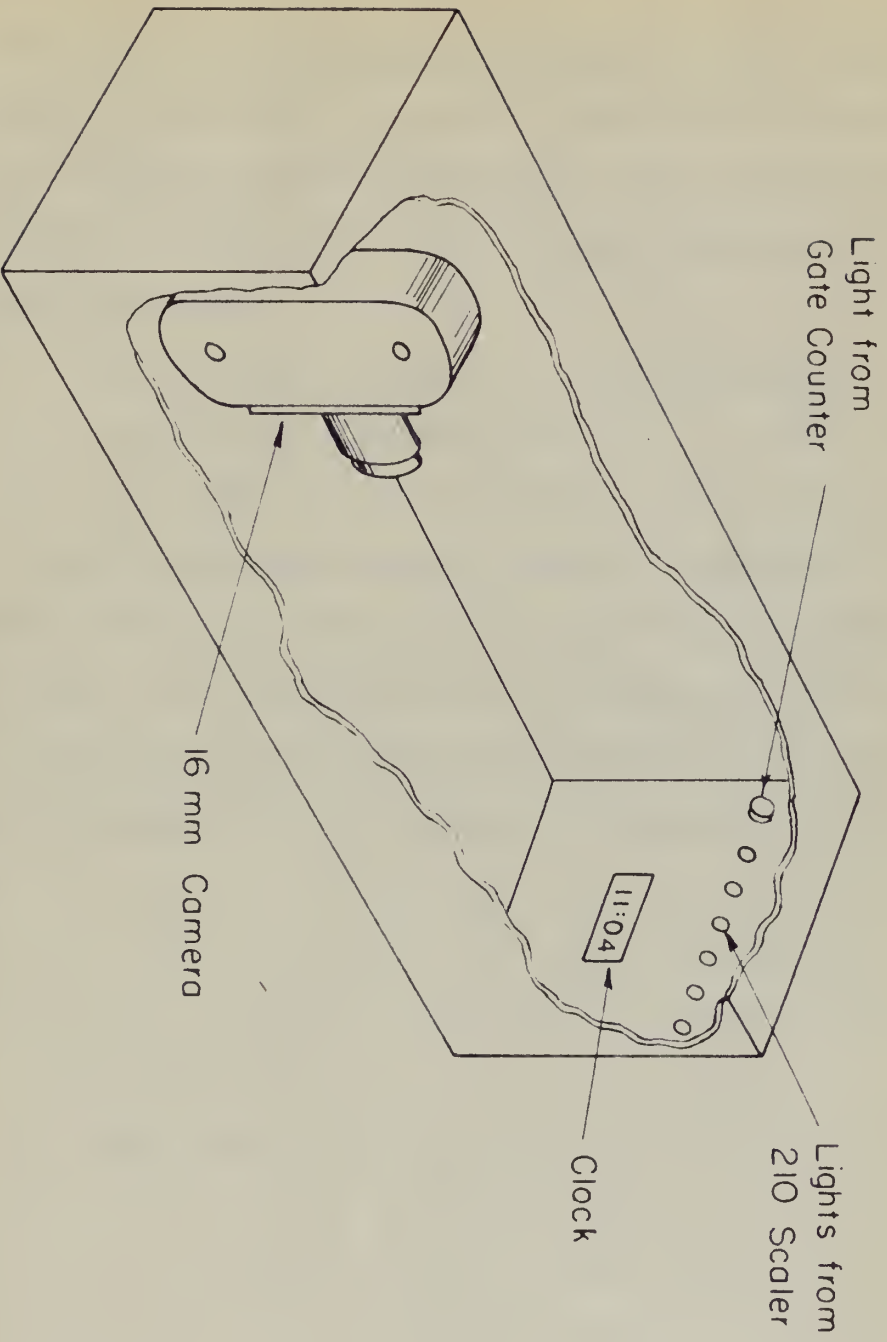
Method of Recording Scaler Lights

The rectangular box shown in the figure is light-tight and a standard 16-mm movie camera, equipped with a short focal length lens, records the fact that the gate was opened and the channel number. The film is externally driven at 9 inches per minute. The clock is for identification of the run.

Figure 8

Method of Recording Carrier Lights

The rectangular box shown in the figure is
light-tight and a standard 16-mm movie
camera, equipped with a short focal length
lens, records the fact that the gate was
opened and the channel number. The film is
automatically driven at 9 inches per minute.
The clock is for identification of the run.



The second method of recording the output of the analyzer is on a set of sixteen mercury registers. Essentially, the binary system of the scaler lights is converted into a scale of sixteen by means of a diode matrix. The sixteen registers can be set (by selector switch) to cover:

- a. Channels 0-15, 16-31, 32-47, ..., 112-127;
- b. Channels 0-31, 32-64, etc; or
- c. Channels 0-63 and 64-127.

Investigation of the overall electronic stability of the spectrometer has shown a drift of the order of 1 percent during a period of one hour. It has been determined that the major part of the drift originates in the addition circuit. The pulse-height analyzer itself is stable to 1 percent over a period of several hours.

The second method of recording the output of the analyzer is on a set of sixteen rotary registers. Essentially, the binary system of the scalar lights is converted into a scale of sixteen by means of a disk matrix. The sixteen registers can be set (by selector switch) to cover:

- a. Channels 0-15, 16-31, 32-47, ... , 112-127;
- b. Channels 0-31, 32-63, etc; or
- c. Channels 0-63 and 64-127.

Investigation of the overall electronic stability of the spectrometer has shown a drift of the order of 1 percent during a period of one hour. It has been determined that the major part of the drift originates in the addition circuit. The pulse-height analyzer itself is stable to 1 percent over a period of several hours.

III. SELECTION OF PAIRS

The principle of selection of pairs created in the converter and rejection of Compton recoil electrons is accomplished by a discriminator in the output of unit No. 2 (D2 of Figure 4). Pairs are mostly emitted in the forward direction with the mean angle of bipartition given to a close approximation²¹ by $\theta_1 = mc^2/E_p$, where $mc^2 = 0.51$ Mev, and E_p = photon energy less 1.02 Mev. The collision energy loss per cm for 1- to 15-Mev electrons is constant within 10 percent if the density effect²³ is included. Hence, to a first approximation, a pair will lose twice as much energy in scintillator No. 2 as will a Compton recoil electron. Therefore, we require that a minimum energy loss be sustained in scintillator No. 2 in order to record a coincidence with scintillator No. 1, resulting in addition of the energy lost by collision in Nos. 1 and 2, and yielding a pulse whose height is linearly proportional to the energy of the incident photon less 1.02 Mev.

For 17-Mev incident x-rays one would expect that D2 would do a good job of separating out the pairs. Figure 9 is an estimate of the pulse-height distribution for the 17.6-Mev incident gamma. Appendix I describes the method of obtaining this figure. One need only set D2 at 1.15-Mev energy loss in order to insure adequate pair selection.

III. SECTION ON PAIRS

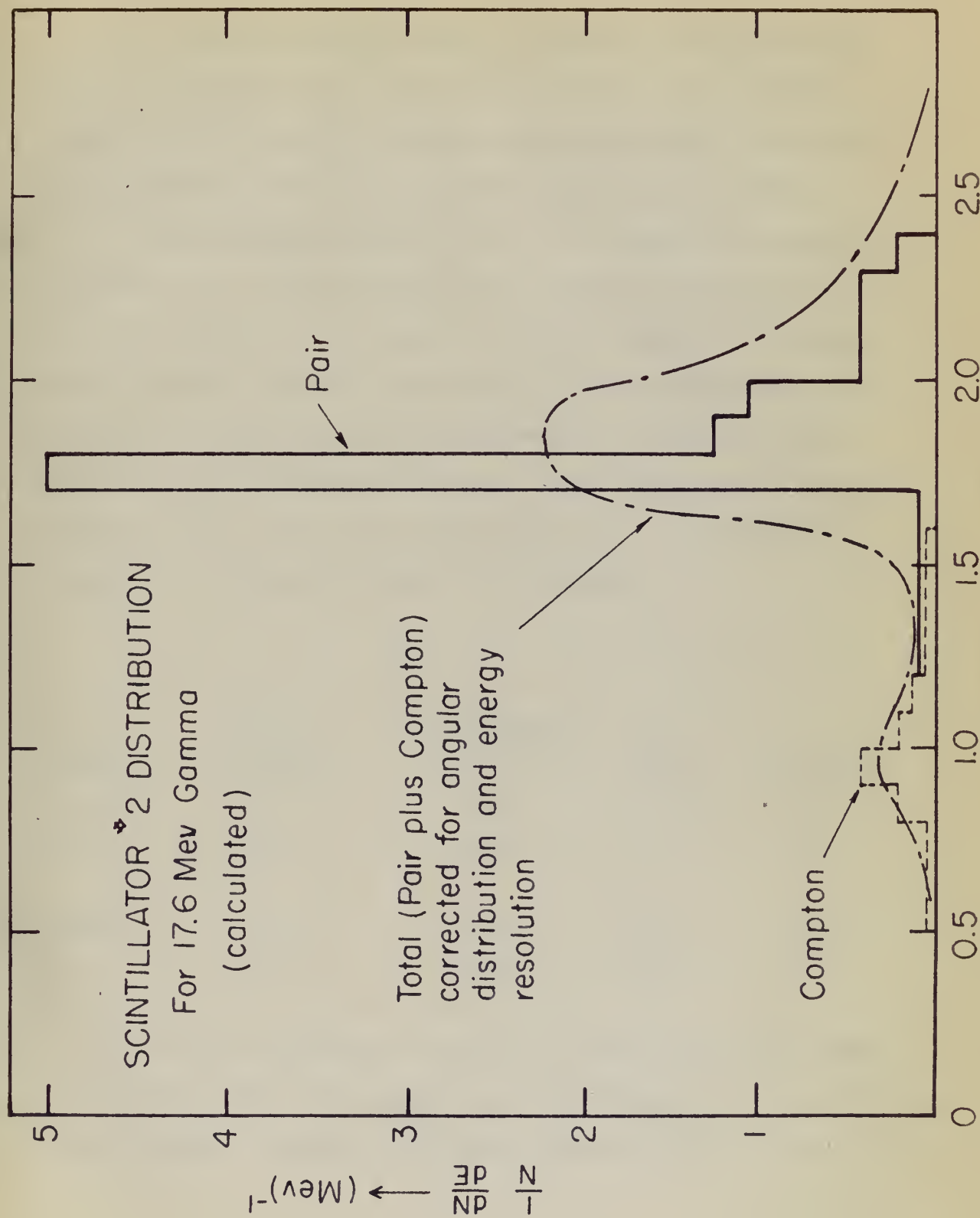
The principle of selection of pairs created in the counter and rejection of certain results is accomplished by a discrimination in the nature of the pairs (see Figure 1). This is usually achieved in the following direction with the same kind of discrimination given as a good approximation $\frac{1}{2} \frac{dN}{dt} = m_0^2 \sqrt{v_0}$, where $m_0^2 = 0.25$ MeV, and $\frac{1}{2} \frac{dN}{dt} =$ photon energy has 1.05 MeV. The collision energy loss per pair is 1.05 MeV electron in collision with in 10 percent of the energy loss is indicated. Thus, as a first approximation, a pair will have about as much energy as the electron. This will be a higher energy electron. Therefore, we require that a minimum energy loss be indicated in selection. This is achieved by a coincidence with selection No. 1, resulting in a selection of the energy loss of collision in Nos. 1 and 2, and yielding a value which is directly proportional to the energy of the incident electron 1.05 MeV.

The 17-MeV incident energy was not known that it would be a good job of separating out the pairs. Figure 2 is an estimate of the pair-creation threshold for the 17-MeV incident energy. Since this I describe the method of obtaining this figure. The need only set up at 1.15-MeV energy loss in order to know whether pair creation.

Figure 9

Calculated Differential Energy Distribution Curves
for Scintillator No. 2, 17.6 Mev, 16-mil Pb Converter

The method of calculation of the curves is explained in Appendix I. The contribution to the distribution by pairs and Compton recoil electrons formed in the scintillator itself has not been taken into account.



At 6 Mev, a worthwhile estimate of the pulse-height distribution for scintillator No. 2 could only be obtained by a detailed "Monte Carlo"¹⁴ calculation, which has not been carried out. It is more difficult to separate the pairs at 6 Mev than at 17 Mev.

Pairs and Compton recoil electrons may originate in scintillators themselves. If these electrons originate in scintillator No. 1, a coincidence will not be recorded. If they originate in the anti-coincidence unit, they will lose enough energy to trigger the anti-coincidence circuit and a coincidence count will not be recorded. However, if these electrons originate in scintillator No. 2, the possibility exists of recording a coincidence count. For comparison purposes, we examine the relative probabilities:

TABLE I

<u>Process</u>	<u>16-mil Lead Converter</u>	<u>Scintillator No. 2</u>	<u>E_{γ}</u>	<u>Reference</u>
Compton	0.7	0.9	6	25
Pair	1.0	0.1	6	44
Compton	0.32	0.39	17	25,29
Pair	2.1	0.25	17	29

Any pairs originating in unit No. 2, which lose enough energy in scintillator No. 2 to trigger D2, will contribute to a sharp resolution function. However, any Compton recoil electrons which are

at 6 Hz, a systematic estimate of the pulse-height distribution for scintillator No. 2 could only be obtained by a detailed "Monte Carlo" calculation, which has not been carried out. It is more difficult to separate the peak at 6 Hz than at 17 Hz. Table III shows results obtained by means of the method described in scintillator No. 1. It was assumed that the estimate of the pulse-height distribution will not be repeated. If they estimate in the anti-coincidence unit, they will have enough energy to trigger the anti-coincidence circuit and a coincidence count will not be repeated. However, it was assumed that the estimate in scintillator No. 2, the probability of recording a coincidence count. For comparison purposes, we assume the relative probabilities:

TABLE I

Scintillator	Y	Scintillator No. 2	10-11 Hz	Scintillator
22	6	0.9	0.7	Scintillator
11	6	0.1	1.3	17 Hz
22, 23	17	0.39	0.32	Scintillator
23	17	0.32	2.1	17 Hz

The anti-coincidence unit is used in this No. 2, which has enough energy in scintillator No. 2 to trigger No. 1, will contribute to a sharp peak in the spectrum. However, any coincidence count obtained with the

multiply scattered in scintillator No. 2 so as to trigger unit No. 2 (increased path length, increased energy loss by ionization) will result in the broadening of the shape of the spectrum, particularly on the low-energy side, because of the continuous Compton distribution. Qualitatively, it is seen that only low-energy Compton recoil electrons have a large probability of multiple scattering which, combined with their larger angle of emission (Appendix I), make this group the most troublesome. Hence, one way of cutting down the low-energy tail resulting from the Compton effect is to raise the bias of D1 or reduce the thickness of scintillator No. 2.

initially contained in amplifier No. 2 so as to return with No. 2 (instead with lamp) increased energy from by feedback will result in the widening of the range of the spectrum, particularly on the low-energy side, because of the continuous down on distribution. Qualitatively, it is seen that only low-energy down would electrons have a large probability of certain scattering which combined with their larger range of action (Appendix 1), with this group the most noticeable. Hence, one way of cutting down the low-energy tail resulting from the constant effect is to raise the bias of 11 or reduce the thickness of amplifier No. 2.

TABLE I
Summary of results of measurements of the energy spectrum of the detector

Energy (eV)	Count rate (cps)	Resolution (eV)	Efficiency (%)
10	100	10	10
20	200	20	20
30	300	30	30
40	400	40	40
50	500	50	50

The above measurements were made with the detector in the low-energy region. The results show that the energy spectrum of the detector is very sensitive to the bias voltage and the thickness of the amplifier. The energy spectrum of the detector is very sensitive to the bias voltage and the thickness of the amplifier.

IV. FUNCTION OF SCINTILLATOR NO. 3.

Up to this point, it has been unnecessary to discuss scintillator No. 3 as the operation of the spectrometer as designed only requires unit No. 1 and unit No. 2, as previously described. At the near surface of scintillator No. 2, there may exist a high-level electron background. Most of these electrons come from the collimator.

For a 17-Mev incident gamma-ray, this large number of scattered electrons is an order of magnitude larger than the number created purposely in the converter. Some of these electrons will lose a sufficient amount of energy in scintillator No. 2 to contribute to the coincidence counting rate.

One can get rid of these electrons either by a magnet or by a third scintillator in anticoincidence. The setting of the discriminator on unit No. 3 is not critical. D3 is set so that a minimum ionizing particle in passing straight through scintillator No. 3 causes the anticoincidence circuit to operate.

IV. POSITION OF ANTENNAE NO. 1.

On this subject, it has been necessary to discuss antenna-
No. 1 in the position of the structure as described only
reference with No. 1 and with No. 2, as previously described. As the
only a series of antennae No. 1, there may exist a high-level
of the antenna. That of these antenna come from the multi-
factor.
For a 12-ray antenna, however, this factor must be multi-
plied also by an order of magnitude larger than the number
of the antenna in the antenna. Some of these antenna will
have a sufficient amount of energy in antenna No. 1 to contri-
bute to the antenna antenna rate.
One and two of these antenna with a series of by
a third antenna in antenna. The setting of the dis-
tribution on with No. 1 is not explicit. It is not as that a mini-
mum having antenna in antenna antenna through antenna No. 1
cause the antenna antenna antenna to operate.

V. RESOLUTION

Ideally, a monochromatic 5- to 17-Mev x-ray will interact with the converter forming pairs and Compton recoil electrons. As previously discussed, scintillation unit No. 2 will discriminate against the Compton recoil electrons, and pairs only will be recorded as coincidence counts, resulting in a single pulse height corresponding to $E_\gamma - 1.02$, where E_γ is incident monoenergetic x-ray energy in Mev. Resolution is defined as the width in Mev at half maximum divided by the peak energy in Mev.

The resolution of this spectrometer is determined by the following factors:

1. Light collection and photomultiplier statistics;
2. Radiation energy loss in the scintillators;
3. Electron escape from the scintillators;
4. Energy loss in the converter;
5. Capture of one or both annihilation quanta.

LIGHT COLLECTION AND PHOTOMULTIPLIER STATISTICS

The absorption of light is small¹⁷ in plastic scintillators, such as "Pilot B." Photomultiplier statistics can be treated in good approximation^{10,31,32} as a statistical fluctuation in the number of photoelectrons at the first dynode of the photomultiplier.

NEWLON • 7

divided by the peak energy in Mev.

The mission of this organization is to educate the public

1. Direction of wave or both oscillation periods.
2. Energy loss in the compound.
3. Direction waves from the oscillators.
4. Radiation energy loss in the oscillators.
5. Light oscillation and photomultiplier statistics.

ALL INFORMATION CONTAINED
HEREIN IS UNCLASSIFIED

per of absorption of the first group of the monomers.

Good agreement ^{10,11,12} as a statistical treatment in the case
such as "Site 2." The statistical treatment can be treated in
the absorption of light in small ¹³ in glass solubility.

Mark and Goldring¹³ have measured the resolution of the Cs¹³⁷ 624-kev internal conversion line, using "Pilot B" scintillator and have obtained a value of 15 percent, as compared with 7 percent for NaI. This result implies an average of about 60 photoelectrons per Mev energy loss in the scintillator.

Using this figure of 60 photoelectrons per Mev energy loss and assuming that the light collection efficiency for scintillator No. 2 is half that for scintillator No. 1, we arrive at the following contributions to the energy resolution of the spectrometer resulting from light collection and photomultiplier statistics:

E_{γ}	Resolution (Percent.)
6	14
10	10
17	7

RADIATION ENERGY LOSS

Electron energy loss by radiation does not contribute to scintillator fluorescence. Bethe and Heitler¹⁴ give the probability, P_{α} , that an electron traversing t radiation lengths will have an energy loss less than α times its initial energy (neglecting loss by ionization) as:

$$P_{\alpha} = \frac{\alpha^{t/\log 2}}{(t/\log 2)!},$$

Mark and Goldring¹² have measured the resolution of the Cs¹³³

50-kev internal conversion line, using "Pilot B" scintillator and have obtained a value of 12 percent, as compared with 7 percent for NaI. This result implies an average of about 50 photoelectrons per keV energy loss in the scintillator.

Using this figure of 50 photoelectrons per keV energy loss and

assuming that the light collection efficiency for scintillator No. 2 is half that for scintillator No. 1, we arrive at the following con-

tribution to the energy resolution of the spectrometer resulting from light collection and photomultiplier statistics:

Resolution (Percent.)	$\frac{E}{Y}$
11	2
10	10
7	17

SCINTILLATOR ENERGY LOSS

Electron energy loss by radiation does not contribute to energy resolution. With and without¹³ the two probabilities, P_1 and P_2 , that an electron traversing a radiation length will have an energy loss less than ϵ times the initial energy (neglecting loss by brems-

strahlung) are

$$P_1 = \frac{\sqrt{2\epsilon}}{1 + \sqrt{2\epsilon}}$$

where t is the thickness in radiation lengths²⁷. A plot of this function for a 10-Mev electron traversing its total range is shown in Figure 10. If ionisation losses and variation of the radiative loss with energy are taken into account³⁵, the effect will be to decrease further the low-energy tail. Examination of the energy distribution of the pairs^{9,15} reveals that the low-energy tail will be further decreased; and, consequently, radiative loss at 17-Mev incident x-ray energy will not appreciably affect the resolution. Pairs from a 6-Mev incident x-ray will have negligible loss by radiation.

ELECTRON ESCAPE

Some of the electrons and positrons may escape from the scintillator. In calculating electron escape probability, the electron or positron was assumed to enter scintillator No. 2 at an average angle θ_0 (see Appendix I). The gaussian approximation of Rossi and Greisen²⁷ for the lateral displacement was graphically integrated taking into account the energy loss by collision. The mean square angle of scattering in the gaussian approximation²⁷ is:

$$\frac{E_s^2 t}{2 p^2 \beta^2},$$

where the meaning of the symbols is given in Appendix I. Thus, we find that a 15-Mev electron has an 18 percent probability of escaping with more than 1.5 Mev. Weighting the escape probability with

where θ is the distance in radians between the two points of view. The function for a 10-ray electron traversing the total range is shown in Figure 10. In calculating losses and variation of the electron loss with energy the value $\theta = 10^\circ$ was used. The effect will be to increase the loss by the factor 1.1. The calculation of the energy distribution of the ions¹² remains the same as for the electron case. The ions are assumed to be uniformly distributed, and the energy loss will be correspondingly altered. With these assumptions the energy loss will have negligible loss by ionization.

REFERENCES

1. The electron and positron range curves from the electron. In calculating electron energy probability, the electron at position was assumed to enter uniformly at $x = 0$ as a source. 2. The electron spectrum of the ion and positron¹² for the lateral dimension was previously indicated. The mean square value of scattering in the electron spectrum¹² is given by the equation:

$$\frac{1}{2} \frac{d^2}{dx^2} \left(\frac{1}{2} \frac{d^2}{dx^2} \right) = \frac{1}{2} \frac{d^2}{dx^2} \left(\frac{1}{2} \frac{d^2}{dx^2} \right)$$

where the constant of the electron is given in Appendix I. Thus, the total electron loss as a function of energy probability of energy loss with mean value 1.2 was. Including the energy probability with

Figure 10

Electron Energy Loss by Radiation

This curve is the differential probability of energy loss by radiation for 100 10-Mev electrons traversing 0.15 radiation lengths in carbon.

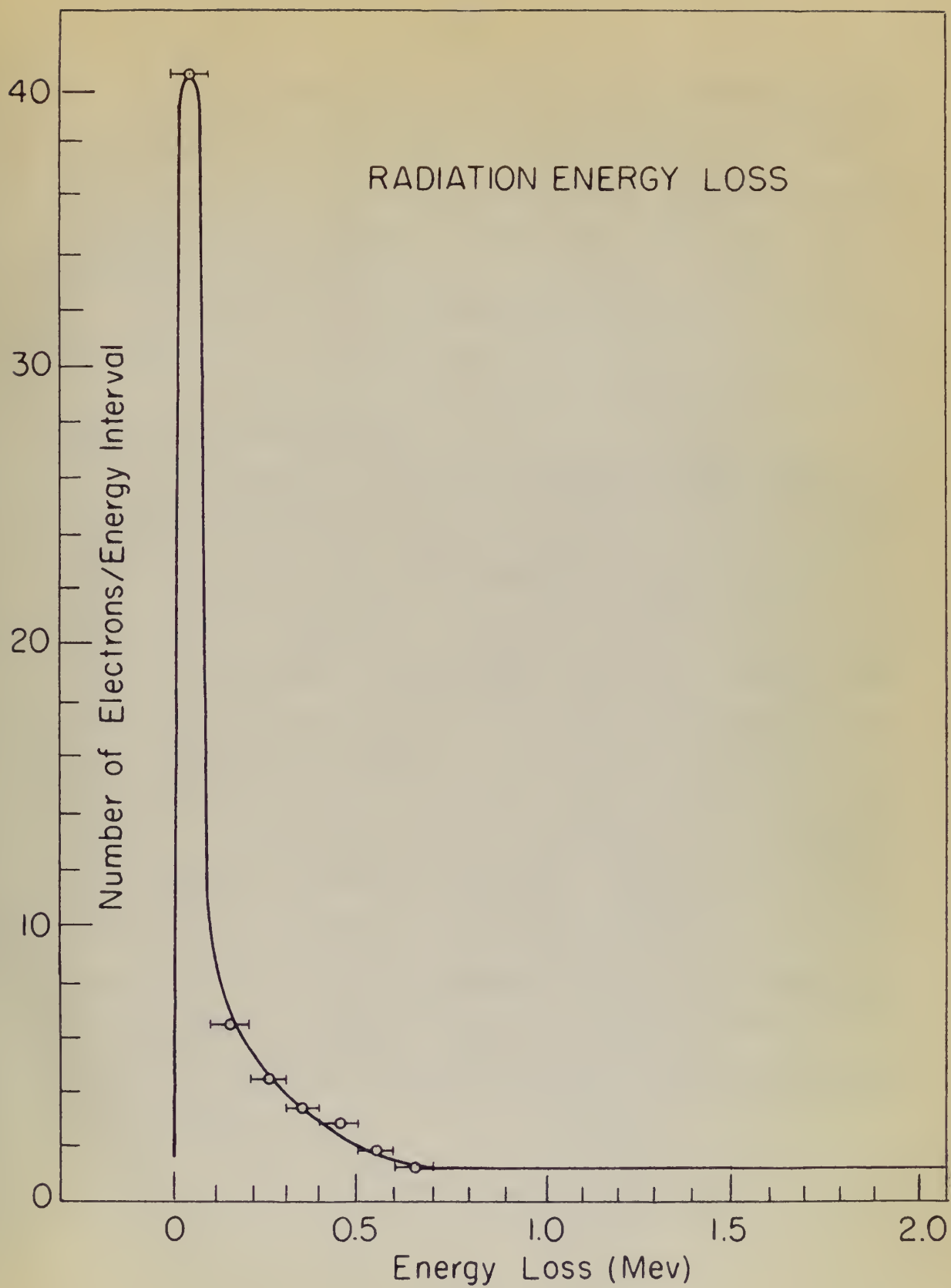
The first of these is the fact that the rate of energy loss by radiation is proportional to the square of the velocity of the particle. This means that the rate of energy loss is much greater for a particle moving at a high velocity than for a particle moving at a low velocity. The second of these is the fact that the rate of energy loss by radiation is proportional to the mass of the particle. This means that the rate of energy loss is much greater for a heavy particle than for a light particle. The third of these is the fact that the rate of energy loss by radiation is proportional to the square of the charge of the particle. This means that the rate of energy loss is much greater for a particle with a large charge than for a particle with a small charge.

Figure 10

Electron Energy Loss by Radiation

This curve is the differential probability of energy loss by radiation for 100 keV electrons traversing 0.15 radiation lengths in carbon.

The curve shows that the probability of energy loss by radiation is highest for a small energy loss and decreases as the energy loss increases. This is because the rate of energy loss by radiation is proportional to the square of the velocity of the particle, and the velocity of the particle is highest for a small energy loss. The curve also shows that the probability of energy loss by radiation is highest for a small mass and decreases as the mass increases. This is because the rate of energy loss by radiation is proportional to the mass of the particle, and the mass of the particle is highest for a small energy loss. Finally, the curve shows that the probability of energy loss by radiation is highest for a small charge and decreases as the charge increases. This is because the rate of energy loss by radiation is proportional to the square of the charge of the particle, and the charge of the particle is highest for a small energy loss.



the pair energy distribution function²⁴ gives the approximate resolution caused by electron escape. This is negligible for a 5-Mev x-ray, of the order of 6 percent for the 17-Mev incident x-ray, and a rapidly increasing function of energy above 15-Mev x-ray energy. The length of scintillator No. 1 is equal to the range³⁶ of a 16-Mev electron.

ENERGY LOSS IN THE CONVERTER

The electron pair created in the converter loses energy in the converter and in the aluminum foil before entering the scintillator. This energy loss is not a constant, and the fluctuations in this energy loss contribute to the energy resolution of the spectrometer. The fluctuation of energy loss occurring when electrons pass through absorbers that are thin compared with their range has been experimentally measured³⁷⁻³⁹ and found to agree with the Landau theory⁴⁰. The net effect of multiple scattering is to increase the relative number of low-energy electrons²⁸. The rms fluctuation in energy loss can be most easily calculated using Yang's Δ correction and assuming the gaussian distribution for the multiple scattering (see Appendix I). Proceeding along these lines, we calculate a root mean square energy loss, which, when divided by the electron energy, gives resolution.

The only energy distribution function²¹ gives the approximate ratio of the number of electrons having a given energy to the total number of electrons. This is negligible for a 2-MeV beam, of the order of 6 percent for the 17-MeV beam²², and a rapidly increasing function of energy above 15-MeV energy. The length of the distribution is equal to the range²³ of a 10-MeV electron.

ENERGY LOSS IN THE CONVERTER

The electron path created in the converter loses energy in the converter and in the electron foil before entering the scintillator. This energy loss is not a constant, and the fluctuations in this energy loss contribute to the energy resolution of the spectrometer. The fluctuations of energy loss contribute when electrons pass through elements that are also covered with their range has been experimentally measured²⁴⁻²⁶ and found to agree with the range theory²⁷. The net effect of multiple scattering is to increase the relative error of low-energy electrons²⁸. The net fluctuation in energy loss can be more easily calculated using Fermi's correction and assuming the Gaussian distribution for the multiple scattering (see Appendix I). Proceeding along these lines, we calculate a root mean square energy loss, which, when divided by the electron energy, gives resolution.

The aluminum foil used to wrap the scintillator has a total thickness of 3 mils. At 6 Mev, the energy loss calculated as outlined above is of the order of 1 percent; at 17 Mev, this loss is negligible.

The converter can be approximated as an electron point source covered with a foil of half converter thickness. The angular distribution of the electrons in pair production will in general have the same effect as multiple scattering; that is, electrons will not travel a constant straight-line path through the foil but will be distributed in direction (hence, path length) according to the pair production angular distribution. Since a characteristic angle of emission (see Appendix I) is inversely proportional to energy, as also is the root mean square angle of scattering, the ratio of these two angles is roughly independent of energy for a given converter thickness. No gain in resolution can be achieved by reducing the converter thickness beyond the point where the root mean square scattering angle becomes equal to the average angle of pair emission.

Assuming an average electron energy equal to one-half ($E_\gamma - 1.02$), where E_γ is incident x-ray energy in Mev, the following results are obtained for a 16-mil lead converter:

<u>E_γ</u>	<u>Resolution (Percent.)</u>
6	14
11	5.7
17	3.5

The aluminum foil used to wrap the metalization has a total thickness of 3 mils. At 6 W, the average loss contained in one inch more is of the order of 1 percent; at 12 W, this loss is negligible.

The converter can be characterized as an electron beam source covered with a foil of half centimeter thickness. The angular distribution of the electrons in this production will be assumed to have the same effect as multiple scattering; that is, electrons will not travel a constant straight-line path through the foil but will be distributed in direction (angle, path length) according to the path production angular distribution. Hence a calculatable angle of emission (see Appendix I) is inversely proportional to energy, as also is the root mean square angle of scattering, the ratio of these two angles is roughly independent of energy for a given converter thickness. No path in scattering can be defined by reducing the converter thickness because beyond the point where the root mean square scattering angle becomes equal to the average angle of path emission.

Assuming an average electron energy equal to 100 eV (E₀ = 100), then E₀ is constant energy in W, the following results are obtained for a 10-mil lead converter:

$\frac{E}{E_0}$	fraction (percent)
1	10
1.2	2.7
1.5	0.2

The effect of radiation loss in the converter is smaller than the above.

CAPTURE OF ANNIHILATION QUANTA

Capture of an appreciable fraction of the annihilation quanta in the scintillator will impair the energy resolution of the spectrometer.

The fraction of gamma-ray energy dissipated by a narrow beam in passing through the scintillator is not the same as the fractional loss of intensity. It is necessary to multiply the probability of each interaction process (Compton and photoelectric) by the probable fraction of the photon energy actually dissipated in the absorber as a result of the process. Using this method, one takes the value of the energy absorption coefficient to be $0.029 \text{ cm}^2/\text{gm}$ at 0.51 Mev for "Pilot B" scintillators (Fano⁴¹).

The method used to calculate the probability that at least one annihilation quantum is absorbed is as follows: Assume an average angle of pair emission and that the range of the electron¹⁸ is approximately that for aluminum. (The energy loss in mica, carbon, and air is not significantly different from that in the same weight of aluminum³³.) From this stopping point, assuming the quanta are isotropically emitted back-to-back with equal energies²¹, we establish an average solid angle and an average path length. From this

The effect of reflection loss in the converter is calculated

the above.

SYSTEM OF ANTENNA POINTS

Customs at an appropriate position of the antenna points

in the calculation will result the energy radiation of the spec-

ification.

The radiation of power-law energy radiation by a source beam

in passing through the antenna is not the same as the radiation

loss of intensity. It is necessary to multiply the probability of

each radiation process (constant and stochastic) by the probability

radiation of the power-law energy radiation in the antenna as

a result of the process. When this method, one takes the value of

the energy radiation coefficient to be 0.009 or 0.01 for

"Also in calculation (Table 1).

The effect loss is calculated the probability that at least

one antenna point is situated is as follows: Assume an aver-

age angle of rays radiation and that the range of the antenna is

approximately that for aluminum. (The energy loss in steel, carbon,

and air is not significantly different from that in the same weight

of aluminum.) From this starting point, assuming the points are

isotropically emitted back-to-back with equal energy, we obtain

that an average solid angle and an average path length. From this

is calculated the average energy absorbed by the scintillator, taking into account the energy distribution function of the pair electrons. At 17 Mev, about 4 percent of the annihilation quanta are absorbed in the scintillator and about 7 percent are absorbed at 6 Mev.

SUMMARY OF EXPECTED RESOLUTION

To summarize this chapter, assuming that the processes above are statistically independent²², one arrives at the following values for the expected resolution of the spectrometer when using a 16-mil lead converter:

<u>E_γ</u>	<u>Resolution</u> <u>(Percent.)</u>
6	20
10	12
17	10

is calculated the energy spread absorbed by the annihilator, taking into account the energy distribution function of the pair electrons. At 17 kev, about 1 percent of the annihilation events are absorbed in the annihilator and about 7 percent are absorbed at 6 kev.

SUMMARY OF EXPERIMENTAL RESULTS

To summarize this chapter, assuming that the processes above are statistically independent, one arrives at the following values for the expected resolution of the spectrometer when using a 10- μ lead converter:

ΔE	Resolution (Fwhm)
17	10
10	12
6	20

VI. CALIBRATION AT THE ROCKEFELLER GENERATOR

The spectrometer is calibrated by using two gamma-rays of known energies to provide the two points necessary to draw the linear characteristics⁹⁻¹¹ of the scintillator. Since there are no available monoenergetic gamma sources about 5 Mev, it is necessary to utilize gamma-rays from nuclear reactions. The source of gamma-rays generally used for this type of work is from the proton bombardment of light elements.

The source of protons for testing the spectrometer was the M.I.T. Rockefeller electrostatic generator. This generator is capable of delivering a magnetically analyzed (to within 0.1 percent) proton beam of 5 microamperes, continuously variable from 0.7 to 4 Mev. The output proton current is determined by a proton beam current integrator. The area of the proton beam at the target is about 4 square millimeters, so that for the purposes of this experiment the gamma-ray originates from a point source. Figure 11 shows a photograph of the spectrometer and proton target. A scale drawing showing distances from the source is given in Figure 1.

In view of the difficulty of preparing thin proton targets that will physically withstand high proton bombardment current, it was decided to use thick targets. Targetholders were made of 10-mil aluminum disks 2 inches in diameter. A 1/16 inch deep 1/2 inch

VI. CALIBRATION OF THE PROTON BEAM

The spectrometer is calibrated by using two types of beam sources to provide the two points necessary to give the linear relationship⁶⁻¹¹ of the voltmeter. Since there are no suitable monochromatic beam sources about 2 MeV, it is necessary to utilize gamma-rays from radium standards. The source of gamma-rays generally used for this type of work is from the isotope of light elements. The source of the spectrum was the U.I.T. Radioactive Spectroscopic Generator. This generator is capable of delivering a continuously varying (to within 0.1 per cent) proton beam of 2 MeV, continuously variable from 0.1 to 1 MeV. The output proton current is determined by a proton beam current integrator. The size of the proton beam at the target is about 1 mm in diameter, so that for the purposes of this experiment the beam may be considered from a point source. Figure 1 shows a photograph of the spectrometer and proton target. A scale drawing showing distances from the source is given in Figure 1.

In view of the difficulty of measuring this proton beam that will typically extend with proton beam current, it was decided to use thick targets. Targets were made of 10-12 mil aluminum disks 1 inch in diameter. A 1/16 inch deep 1/2 inch

Figure 11

The Spectrometer in Place at the MIT Rockefeller Generator

This figure is a photograph of the spectrometer at the Rockefeller generator as it was located for testing and calibration. The proton target is shown in the right of the photograph.

The spectrum of the hydrogen atom is well known. It consists of a series of discrete lines, the wavelengths of which are given by the formula

$$\frac{1}{\lambda} = R \left(\frac{1}{n^2} - \frac{1}{m^2} \right)$$

where R is the Rydberg constant, n and m are integers, and λ is the wavelength. The lines are named after the discoverer of each series: Lyman, Balmer, Paschen, Brackett, and Pfund. The Lyman series is in the ultraviolet, the Balmer series is in the visible region, and the others are in the infrared.

The spectrum of the hydrogen atom is well known. It consists of a series of discrete lines, the wavelengths of which are given by the formula

$$\frac{1}{\lambda} = R \left(\frac{1}{n^2} - \frac{1}{m^2} \right)$$

where R is the Rydberg constant, n and m are integers, and λ is the wavelength. The lines are named after the discoverer of each series: Lyman, Balmer, Paschen, Brackett, and Pfund. The Lyman series is in the ultraviolet, the Balmer series is in the visible region, and the others are in the infrared.

Figure 11

The spectrum of the hydrogen atom is well known. It consists of a series of discrete lines, the wavelengths of which are given by the formula

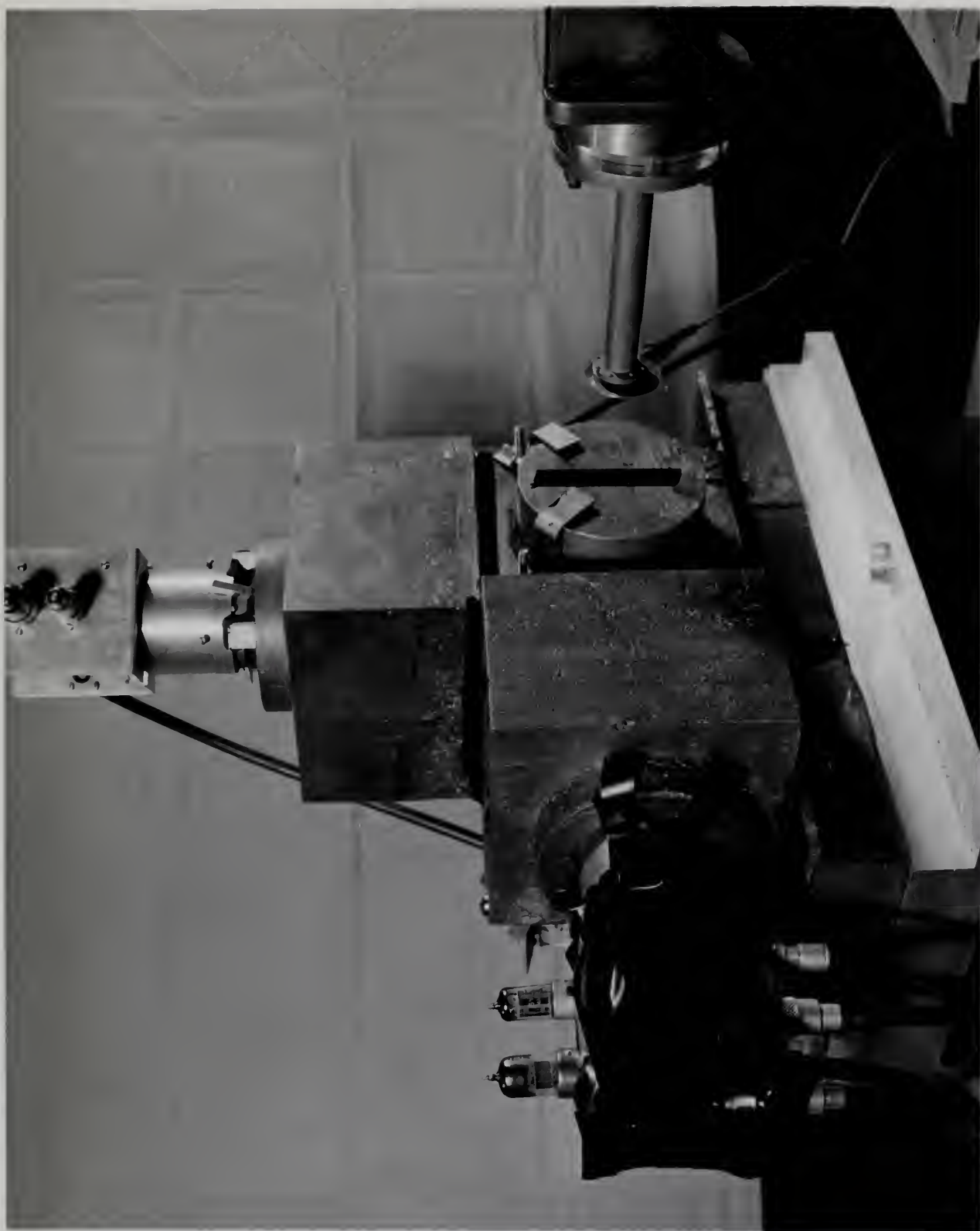
$$\frac{1}{\lambda} = R \left(\frac{1}{n^2} - \frac{1}{m^2} \right)$$

where R is the Rydberg constant, n and m are integers, and λ is the wavelength. The lines are named after the discoverer of each series: Lyman, Balmer, Paschen, Brackett, and Pfund. The Lyman series is in the ultraviolet, the Balmer series is in the visible region, and the others are in the infrared.

The spectrum of the hydrogen atom is well known. It consists of a series of discrete lines, the wavelengths of which are given by the formula

$$\frac{1}{\lambda} = R \left(\frac{1}{n^2} - \frac{1}{m^2} \right)$$

where R is the Rydberg constant, n and m are integers, and λ is the wavelength. The lines are named after the discoverer of each series: Lyman, Balmer, Paschen, Brackett, and Pfund. The Lyman series is in the ultraviolet, the Balmer series is in the visible region, and the others are in the infrared.



diameter recess was formed in the center of the aluminum disk to hold the target material. Using the same die used to make the depression, the target material was pressed into the recess. This method proved satisfactory for all materials other than boron. The B_4C sample was obtained through the courtesy of Professor J. T. Norton, Metallurgical Department, M. I. T. It was in the form of a 3/16 inch thick sample, hot pressed in a graphite die.

A list of energy standards used and references giving the yields and gamma-ray energies follows:

TABLE II

<u>Target Material</u>	<u>Proton Bombardment Energy (Mev)</u>	<u>Gamma Energy (Mev)</u>	<u>Yield ($\gamma/10^9$ Protons)</u>	<u>Reference</u>
B_4C	1.2	16.7	2	12
		12.12	4	12
		4.41	4	12
CaF	1.15	6.13	500	4,12
		7.0	200	4,12
Li Metal	1.15	17.6	20	4,16
		14.8	30	4,16

To a first approximation, the counting rate of the spectrometer is the fraction of solid angle subtended times the probability

discharge process was found in the center of the aluminum disk to hold the target material. During the same die used to make the depression, the target material was pressed into the recess. This method proved satisfactory for all materials other than boron. The B_{10} sample was obtained through the courtesy of Professor J. T. Horton, Metallurgical Department, U. I. T. It was in the form of a $3/16$ inch thick sample, hot pressed in a graphite die. A list of energy standards used and references giving the

values and gamma-ray energies follows:

TABLE II

Reference	Yield ($\mu\text{Ci/g}$) ($\mu\text{Ci/g}$)	Gamma Energy (MeV)	Gamma Decay Constant (hr^{-1})	Target Material
12	2	12.7	1.2	B_{10}
12	1	12.75		
12	1	11.1		
12, 12	200	6.13	1.12	Cu
12, 12	200	7.0		
12, 12	20	17.6	1.12	Al metal
12, 12	30	11.8		

To a first approximation, the counting rate of the spectrum over in the fraction of solid angle subtended times the probability

of producing a pair in the converter times the rate of emission of gamma radiation. The actual efficiency of the counter must be determined by experiment, since the efficiency is an unknown function of D2 and D1 settings, as well as the incident x-ray energy.

Taking into consideration target conditions, pair cross section, and solid angle which obtain at the Rockefeller generator, it was determined that the approximate times to record 1000 counts are as follows:

<u>Target</u>	<u>Time</u>
CaF	10 min
Li	1 hour
B ₄ C	1 hour

The danger of contaminating the Rockefeller generator imposes a proton current limitation when bombarding lithium targets; this limitation is not present with B₄C. This fact, coupled with the formation of LiOH at the surface, reduces the maximum attainable lithium yield by about a factor of 10, which effectively gives the same obtainable counting rate for lithium and boron.

of producing a pair in the counter from the rate of a pair of
 from the counter. The actual efficiency of the counter must be
 determined by experiment, since the efficiency is an important function
 of the rate of the counter, as well as the incident x-ray energy.
 The counter was operated under constant conditions, but when the
 rate was varied, the efficiency was also varied. The efficiency was
 determined from the experiment and the efficiency was found to be
 as follows:

Rate (pairs/sec)	Efficiency (%)	Time (min)
10	10	10
100	10	10
1000	10	10

The counter of construction the counter generator is
 a proton counter which is used for the detection of the
 radiation is not known with 100% efficiency, coupled with the for-
 mation of the counter, the counter is not able to detect the
 yield by about a factor of 10, which effectively gives the same ob-
 servable counting rate for lithium and boron.

1000	100	100
100	10	10
10	1	1

VII. DISCUSSION OF EXPERIMENTAL RESULTS

ENERGY CALIBRATION

The calibration of the spectrometer is in terms of the pulser voltage. The raw data are, however, recorded in terms of channel number. The channel number (C) is related to voltage by:

$$C = f(V_{1a} + K'V_{2a}) \quad (1)$$

where V_{1a} and V_{2a} are input pulse heights in volts to the addition circuit from units Nos. 1 and 2, respectively; K' is an amplification factor determined by the parameters of the addition circuit. Assuming linearity as far as the addition circuit, equation (1) may be written:

$$C = g(V)$$

where $V = 3(V_1 + KV_2)$; V_1 and V_2 are the output voltage of scintillation units Nos. 1 and 2, respectively. V is a pulser voltage, and the factor of 3 comes from the parameters of the circuit in which pulser and photomultiplier signals are mixed.

A typical calibration curve, giving $C = g(V)$, is shown in Figure 12. The calibration curve is measured both with $V_2 = 0$ and $V_1 = V_2$ in order to determine the addition factor K . The value of K ordinarily used was 0.450 and was stable to 0.5 percent for several hours. The nonlinearity at the upper end of the curve shown in

VII. INTRODUCTION OF EXPERIMENTAL RESULTS

EXPERIMENTAL CALIBRATION

The calibration of the spectrometer is in terms of the

pulsar voltage. The raw data are, however, recorded in terms of channel number. The channel number (n) is related to voltage by:

$$(1) \quad 0 = 1(V_{1a} + K_1 V_{2a})$$

where V_{1a} and V_{2a} are input pulse heights in volts to the addition circuit from units Nos. 1 and 2, respectively; K_1 is an amplification factor determined by the components of the addition circuit.

Assuming linearity as for an addition circuit, equation (1) may be written:

$$0 = K(V)$$

where $V = 3(V_1 + K_2 V_2)$; V_1 and V_2 are the output voltage of addition units Nos. 1 and 2, respectively. V is a pulsar voltage, and the factor of 3 comes from the geometry of the circuit in which

pulsar and photomultiplier signals are mixed.

A typical calibration curve, giving $0 = g(V)$, is shown in

Figure 12. The calibration curve is measured with $V_2 = 0$ and

$V_1 = V$ in order to determine the addition factor K . The value of

K ordinarily used was 0.450 and was stable to 0.2 percent for sev-

eral hours. The nonlinearity at the upper end of the curve shown in

Figure 12

Calibration Curve

Shown here is a typical calibration curve made before, during, and after each run.

Raw data are in the form of counts per channel as a function of channel number. Data are converted into counts per volt as a function of pulser voltage.

The following is the description of the test:

1. The test is performed in a room with a temperature of 20°C.

$$(2) \quad \frac{1}{\rho} = \frac{1}{\rho_0} + \frac{1}{\rho_1} + \frac{1}{\rho_2} + \dots$$

where ρ is the density of the mixture, ρ_0 is the density of the first component, ρ_1 is the density of the second component, and so on.

Calculation of the density of the mixture

There are two methods for calculating the density of the mixture:

1. The first method is to use the following formula:

2. The second method is to use the following formula:

3. The third method is to use the following formula:

4. The fourth method is to use the following formula:

5. The fifth method is to use the following formula:

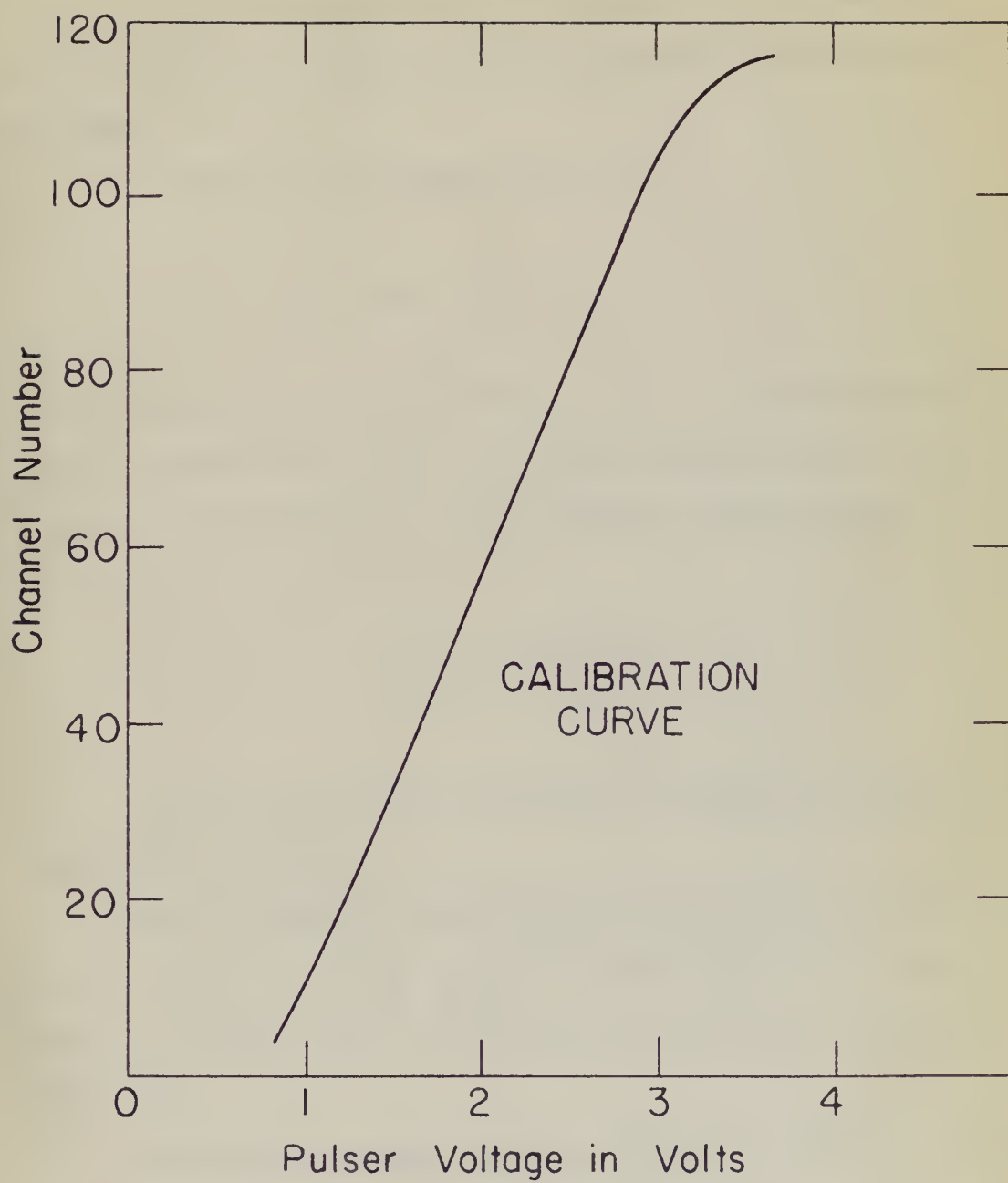


Figure 12 comes from overloading the stage of amplification just before the pulse-height analyzer. The nonlinearity in the lower part of the curve comes from diode nonlinearity in the pulse-height analyzer.

The energy of the incident x-ray is:

$$E_{\gamma} = 1.02 + E_1 + E_2 + E_0 ,$$

where E_1 and E_2 are energy losses (in Mev) in scintillators Nos. 1 and 2, respectively, and E_0 is the most probable energy lost by electrons and positrons in the lead converter (about 0.5 Mev).

$$V = \frac{V_1}{E_1} E_1 + K \frac{V_2}{E_2} E_2 .$$

The ratios V_1/E_1 may be controlled by varying the photomultiplier high voltage.

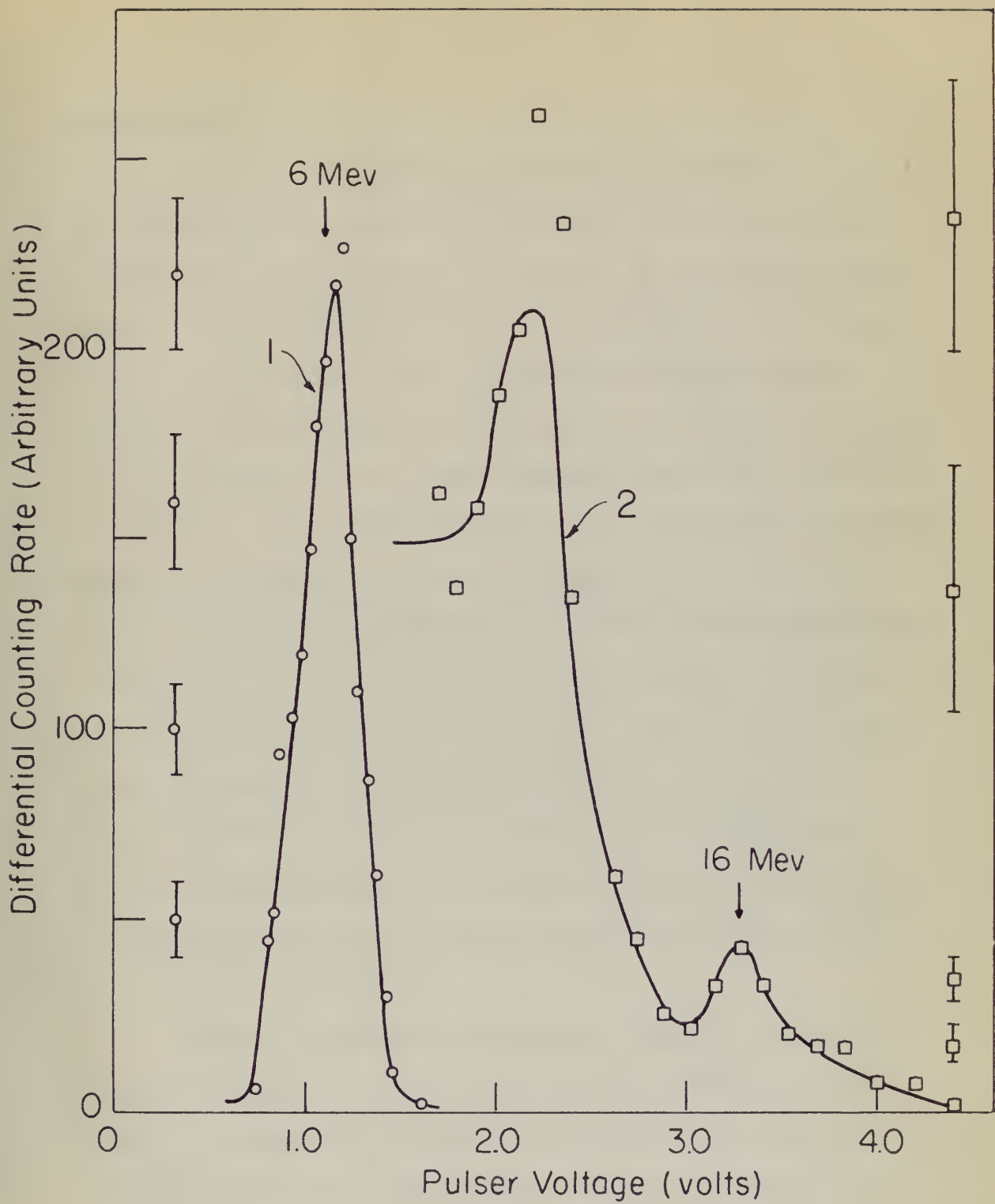
The same negative power supply furnished the high voltage for No. 1 and No. 2. This supply was stable to 0.1 percent for periods of several hours. Both photomultipliers were operated at -740 volts.

Calibration was accomplished by varying the addition factor, K , until the peaks from the 6-Mev fluorine line and the 16-Mev B_4C line fell in the correct relative positions (see Figure 13).

Figure 13

Energy Calibration

Curve No. 1 was obtained by proton bombardment of a thick CaF target; curve No. 2 by proton bombardment of a thick B_4C target. A 16-mil lead converter was used for both curves. The boron curve (No. 2) from 1.5 - 2.5 volts was obtained with poor statistics and normalized to match the 2.5 - 4.5 volt section. There is some evidence of the 12-Mev line at 2.3 volts. The anticoincidence circuit had not been designed when these runs were made.



FLUORINE RUMS

The low-energy limitation of the spectrometer is imposed by the rapid decrease of the pair production cross section with decreasing energy, combined with the increase in Compton cross section. At about 5 Mev (where these two cross sections are about equal), the resolution of the spectrometer is limited by the inability of discriminator No. 2 to perform its designed function; that is, separation of the doubly ionizing pulses of the pair process from the singly ionizing pulses of the Compton recoil electrons. Figure 14 illustrates the lack of a definite separation between pairs and Compton recoil electrons for 6-Mev incident x-ray energy. A sufficiently thin converter with a very thin scintillator No. 2 would perform this function at, say, 3 Mev, since multiple scattering in the converter and in the scintillator, with consequent increased fluctuations in the energy loss, would be minimized. A point is reached, however, where light collection difficulties and photomultiplier statistics impose a lower energy limit to the usefulness of the spectrometer.

Figure 15 illustrates the effect of changes in spectrum shape with changes in D1. In order for the spectrometer to function, it is necessary that there be a region where changing D1 does not materially affect spectrum shape. Figure 15 illustrates that such a plateau does in fact exist; that is, changing D1 from very

DISCUSSION

The low-energy limit of the spectrometer is imposed by

the rapid decrease of the pair production cross section with de-
creasing energy, combined with the increase in Compton cross sec-
tion. At about 5 keV (where these two cross sections are about

equal), the resolution of the spectrometer is limited by the
stability of discriminator No. 2 to perform the desired function;
that is, separation of the doubly ionizing peaks of the pair pro-
cess from the singly ionizing peaks of the Compton recoil electrons.

Figure 11 illustrates the lack of a definite separation between
pair and Compton recoil electrons for 6-MeV incident x-ray energy.

A sufficiently thin converter with a very thin collimator No. 2
would perform this function at, say, 3 MeV, since multiple scatter-
ing in the converter and in the collimator, with consequent in-
creased fluctuations in the energy loss, would be minimized. A

point is noted, however, where light collection efficiencies and
photoelectron statistics impose a lower energy limit to the use-

fulness of the spectrometer.

Figure 12 illustrates the effect of changes in spectrum
shape with changes in E₁. In order for the spectrometer to func-
tion, it is necessary that there be a region where changing E₁ does
not materially affect spectrum shape. Figure 12 illustrates that
such a plateau does in fact exist; that is, changing E₁ from very

Figure 14

Pulse-Height Distribution for Scintillator No. 2 at 6 Mev

This curve was obtained by the proton bombardment of a thick CaF target using a 16-mil lead converter. The standard statistical errors of the points are indicated to the right of the curve.

The following is a summary of the results of the investigation into the causes of the recent economic depression in the United States. It is based on a study of the various factors which have been suggested by different writers, and on a comparison of the results of the investigation with the results of the investigation conducted by the Federal Reserve Board in 1907. The results of the investigation are as follows: (1) The causes of the depression are not due to any one single factor, but to a combination of several factors. (2) The most important factors are the overproduction of goods, the excessive supply of money, and the excessive supply of credit. (3) The overproduction of goods is due to the fact that the production of goods has increased more rapidly than the demand for goods. (4) The excessive supply of money is due to the fact that the money supply has increased more rapidly than the demand for money. (5) The excessive supply of credit is due to the fact that the credit supply has increased more rapidly than the demand for credit.

APPENDIX

The following is a summary of the results of the investigation into the causes of the recent economic depression in the United States. It is based on a study of the various factors which have been suggested by different writers, and on a comparison of the results of the investigation with the results of the investigation conducted by the Federal Reserve Board in 1907. The results of the investigation are as follows: (1) The causes of the depression are not due to any one single factor, but to a combination of several factors. (2) The most important factors are the overproduction of goods, the excessive supply of money, and the excessive supply of credit. (3) The overproduction of goods is due to the fact that the production of goods has increased more rapidly than the demand for goods. (4) The excessive supply of money is due to the fact that the money supply has increased more rapidly than the demand for money. (5) The excessive supply of credit is due to the fact that the credit supply has increased more rapidly than the demand for credit.

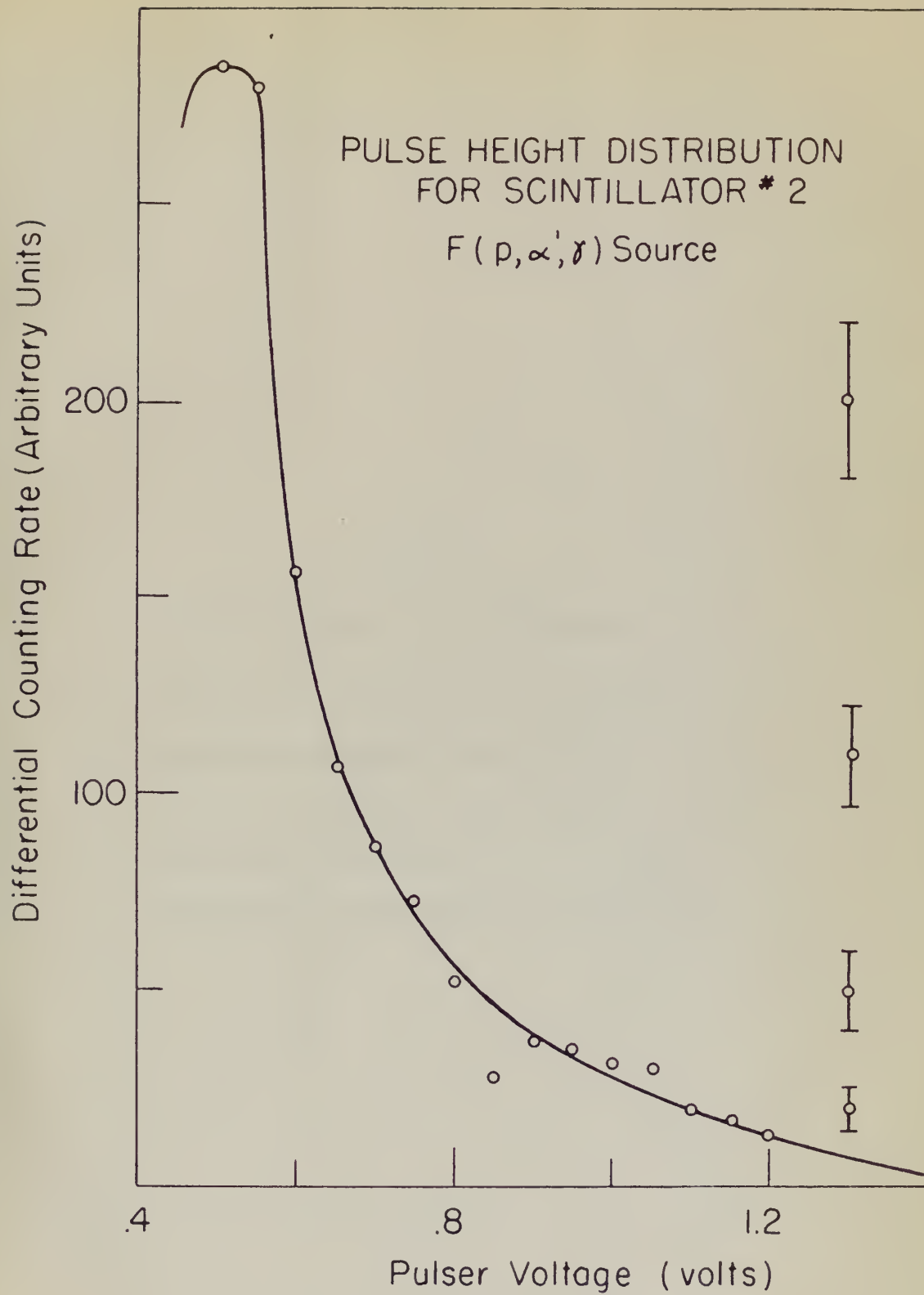


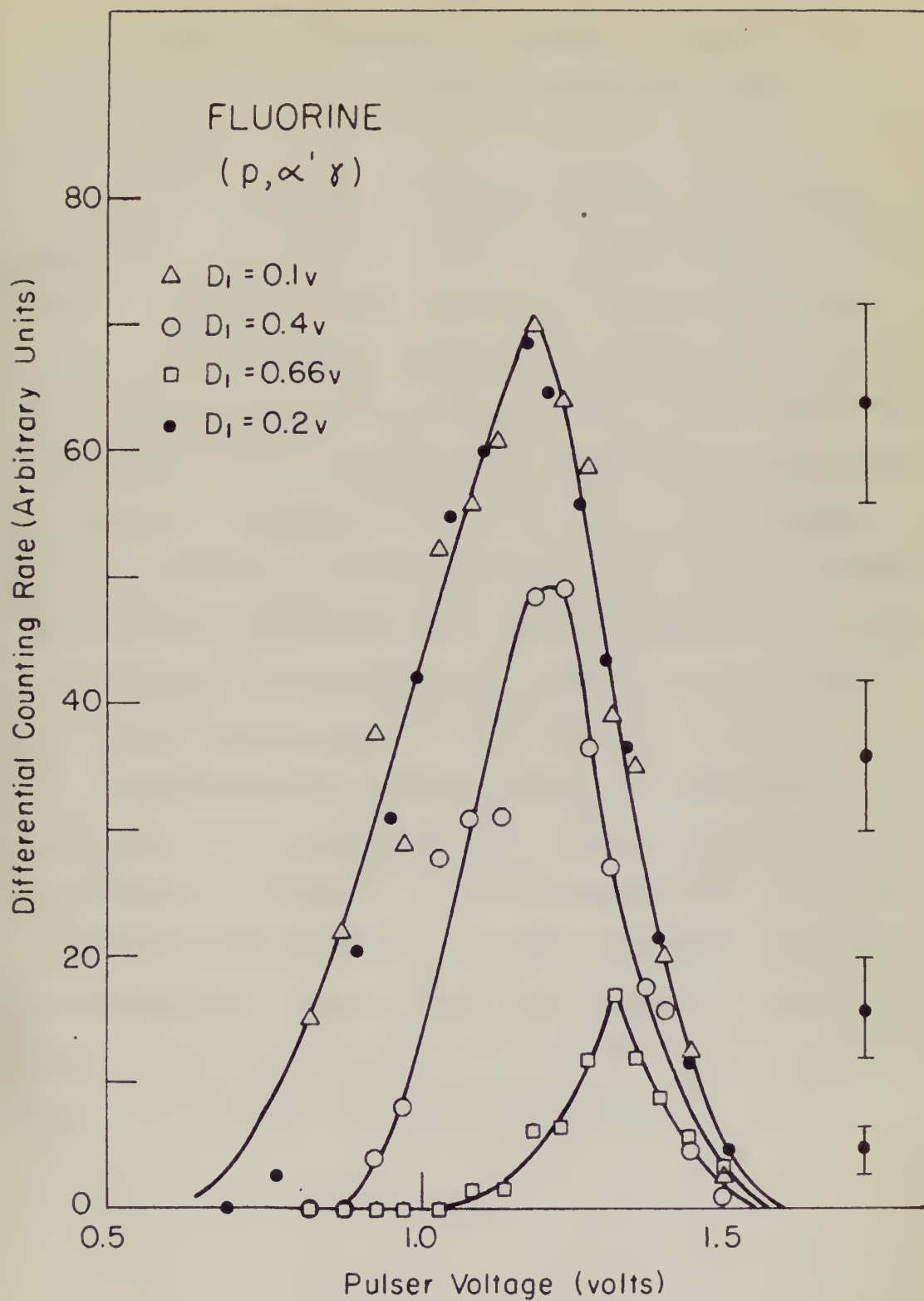
Figure 15

Effect of Changing Discriminator No. 1

All curves in this figure were obtained by proton bombardment of a thick CaF target using a 16-mil lead converter. These curves are normalized to the same number of protons incident on the target.

Figure 12

Effect of changing dimensions No. 1
All curves in this figure were obtained
in a vacuum treatment of a steel bar
subjected to a 1000 lb. load.
These curves are normalized to the same
number of points incident on the target.



low to 0.2 volts does not affect the position of the peak or the resolution. D1 at 0.2 volts requires at least 1-Mev energy loss in scintillator No. 1.

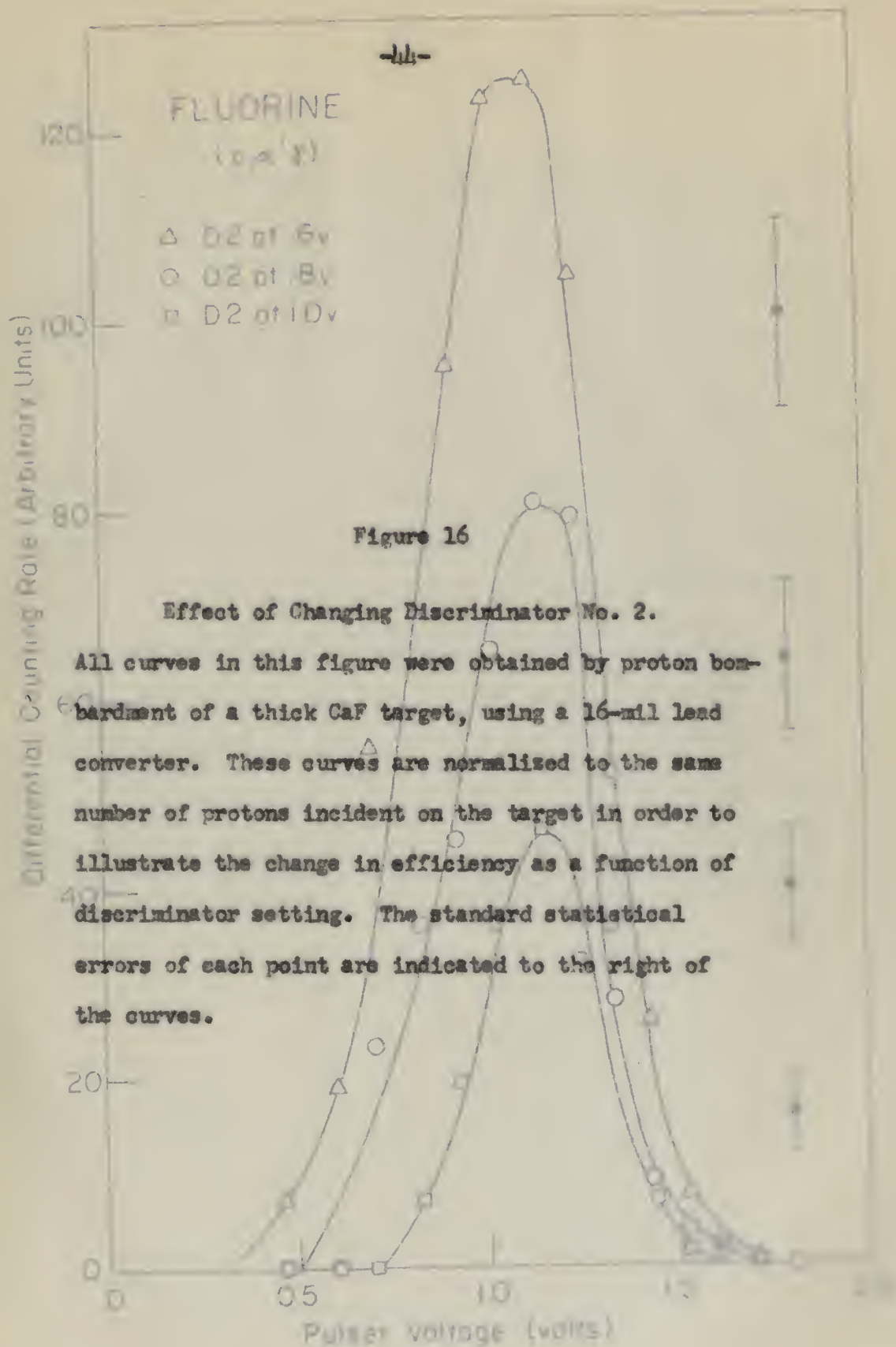
Figure 16 illustrates the change in efficiency of the spectrometer with changes in the setting of discriminator No. 2 at 6-Mev incident x-ray energy. These curves were all made with the same setting of D1; that is, 0.2 volts, and normalized to the same number of protons incident on the $F^{19}(p,\alpha'\gamma)$ target. Hence, the ratio of the areas under the curves of Figure 16 gives directly the ratio of spectrometer efficiency for the given discriminator settings. These ratios are 1:2:3.8, in agreement with the shape of the distribution curve for scintillator No. 2 shown in Figure 11. The curve for D2 = 0.8 volts corresponds to an efficiency of 8×10^{-3} for 6-Mev incident x-ray energy, 16-mil lead converter.

Considering the contribution of the 7-Mev fluorine line, the resolution at 6 Mev is about 25 percent, which is about the resolution predicted in Chapter V. The lowest energy at which the present spectrometer is useful is 6 Mev. To reduce this limit, to improve the resolution at 6 Mev, and perhaps more important to obtain a better plateau of efficiency as a function of D2 would require a thinner lead converter and a thinner scintillator No. 2.

low to 0.2 volts does not affect the position of the peak or the resolution. If at 0.2 volts requires at least 1-mev energy loss in scintillator No. 1.

Figure 10 illustrates the change in efficiency of the spectrometer with changes in the setting of discriminator No. 2 at 6-mev incident x-ray energy. These curves were all made with the same setting of DI, that is, 0.2 volts, and normalized to the same number of photons incident on the ^{137}Cs target. Hence, the ratio of the areas under the curves of Figure 10 gives directly the ratio of spectrometer efficiency for the given discriminator settings. These ratios are 1:1.3:1.8, in agreement with the slope of the distribution curve for scintillator No. 2 shown in Figure 11. The curve for DI = 0.2 volts corresponds to an efficiency of 8×10^{-3} for 6-mev incident x-ray energy, 10-mev lead converter.

Considering the contribution of the 7-mev line, the resolution at 6 mev is about 25 percent, which is about the resolution predicted in Chapter V. The lowest energy at which the spectrometer is useful is 6 mev. To reduce this limit, to improve the resolution at 6 mev, and thereby more important to obtain a better picture of efficiency as a function of E would require a thinner lead converter and a thinner scintillator No. 2.



low to 0.2 volts does not affect the position of the peak or the resolution. DI at 0.2 volts requires at least 1-mev energy loss in scintillator No. 1.

Figure 10 illustrates the change in efficiency of the spectrometer with changes in the setting of discriminator No. 1 at 0-mev incident x-ray energy. These curves were all made with the same setting of DI that is, 0.2 volts, and normalized to the same number of pulses incident on the ^{137}Cs source. Hence, the ratio of the areas under the curves of Figure 10 gives directly the ratio of spectrometer efficiency for the given discriminator settings. These ratios are 1:0.33, in agreement with the ratio of the discriminator curves for scintillator No. 2 shown in Figure 11. The curve for DI = 0.2 volts corresponds to an efficiency of 3×10^{-3} for 0-mev incident x-ray energy, 10-mil lead converter. Considering the contribution of the 7-mev fission line, the resolution at 0 mev is about 97 percent, which is about the resolution predicted in Chapter V. The lowest energy at which the present spectrometer is useful is 0 mev. To reduce this limit, to improve the resolution at 0 mev, and perhaps more important to obtain a better picture of efficiency as a function of E would require a thinner lead converter and a thinner scintillator No. 2.

Figure 16

Effect of Changing Discriminator No. 2.

All curves in this figure were obtained by proton bombardment of a thick CaF target, using a 16-mil lead converter. These curves are normalized to the same number of protons incident on the target in order to illustrate the change in efficiency as a function of discriminator setting. The standard statistical errors of each point are indicated to the right of the curves.

The first series of curves was obtained by the use of the
method described in the preceding section. It is not possible to obtain
curves of this type by the use of the method described in the preceding
section.

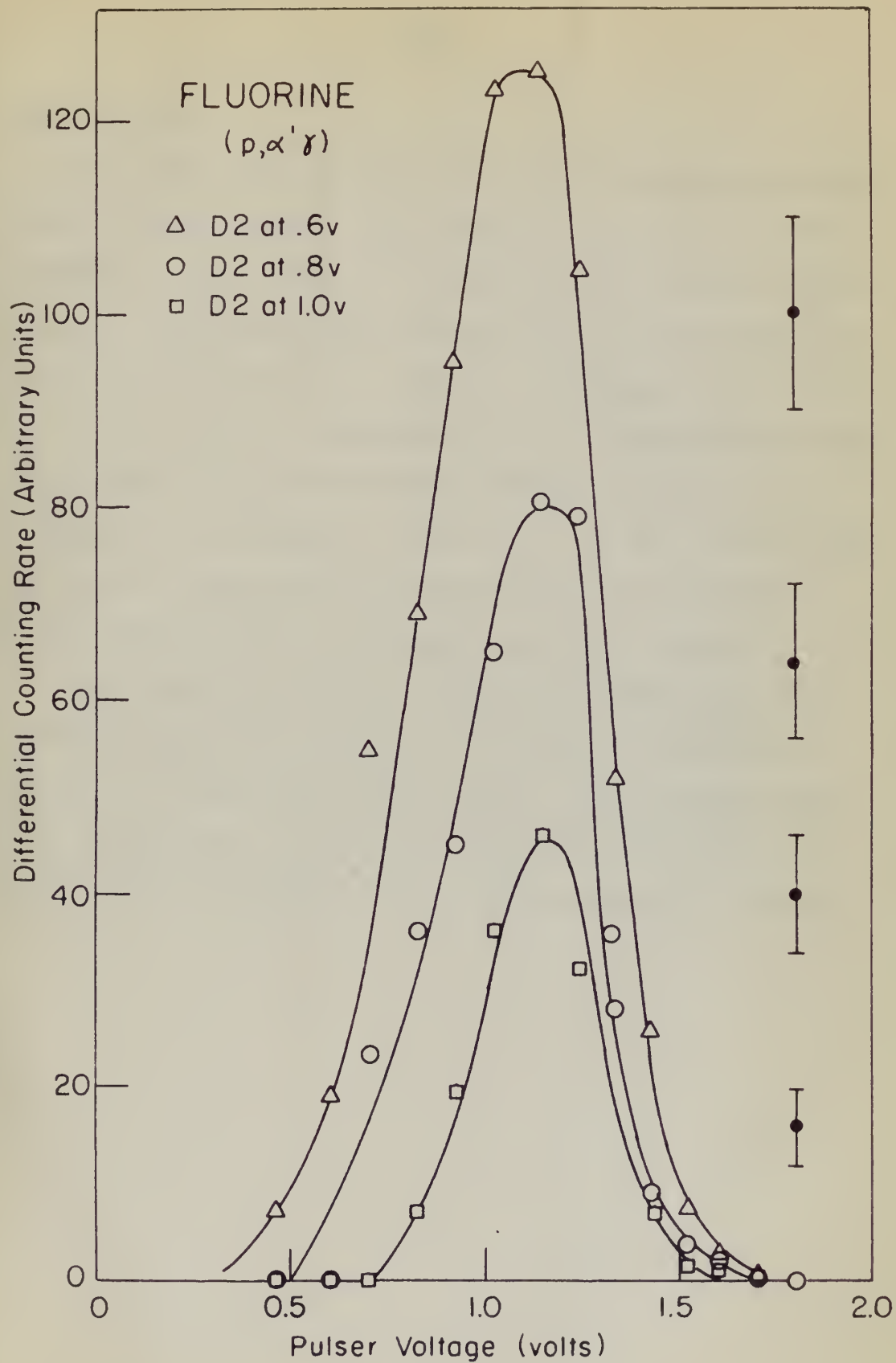
The second series of curves was obtained by the use of the
method described in the preceding section. It is not possible to obtain
curves of this type by the use of the method described in the preceding
section. The curves obtained by the use of the method described in the
preceding section are of the type shown in Figure 1. The curves
obtained by the use of the method described in the preceding section
are of the type shown in Figure 2.

Effect of Temperature on the Curves

All curves in this figure were obtained by the use of the
method described in the preceding section. The curves obtained by the
use of the method described in the preceding section are of the type
shown in Figure 1. The curves obtained by the use of the method
described in the preceding section are of the type shown in Figure 2.
The curves obtained by the use of the method described in the
preceding section are of the type shown in Figure 3. The curves
obtained by the use of the method described in the preceding section
are of the type shown in Figure 4. The curves obtained by the use
of the method described in the preceding section are of the type
shown in Figure 5. The curves obtained by the use of the method
described in the preceding section are of the type shown in Figure 6.

The Curves

The curves obtained by the use of the method described in the
preceding section are of the type shown in Figure 1. The curves
obtained by the use of the method described in the preceding section
are of the type shown in Figure 2. The curves obtained by the use
of the method described in the preceding section are of the type
shown in Figure 3. The curves obtained by the use of the method
described in the preceding section are of the type shown in Figure 4.



HIGH-ENERGY RUNS

The difficulties apparent in the high-energy region, as illustrated by Figure 13, led to the necessity for design of the anticoincidence circuit. Figure 17 illustrates the difficulty in distinguishing singly and doubly ionizing events with the anticoincidence scintillator out of the circuit. This figure also demonstrates the apparent success of scintillator No. 3 in eliminating high background effects which mask the expected doubly ionizing peak calculated and shown on Figure 9 of Chapter III. To date, the only runs made with the anticoincidence unit in operation were the pulse-height distribution in scintillator No. 2 shown in Figure 17.

The prediction in Chapter V regarding electron escape and radiation loss from scintillator No. 1 should be experimentally verified by a high-energy electron source. The high-energy limit of the spectrometer is imposed as a result of rapidly increasing electron escape probability with increasing energy above 15 Mev.

HIGH-ENERGY RAYS

The distribution spectrum in the high-energy region, as illustrated by Figure 11, led to the necessity for design of the end-collector circuit. Figure 12 illustrates the difficulty in this region due to the high-energy region and the end-collector circuit. The figure also demonstrates the apparent necessity of collector No. 2 in eliminating high back-ground counts which may be caused by the high-energy region. It is noted and shown on Figure 2 of Chapter III. In fact, the only way to deal with the end-collector unit in operation were the following distribution in collector No. 2 shown in Figure 13.

The position in Chapter V regarding electron escape and radiation loss from collector No. 1 should be experimentally verified by a high-energy electron source. The high-energy limit of the spectrum is known as a result of rapidly increasing electron escape probability with increasing energy above 15 Mev.

Figure 17

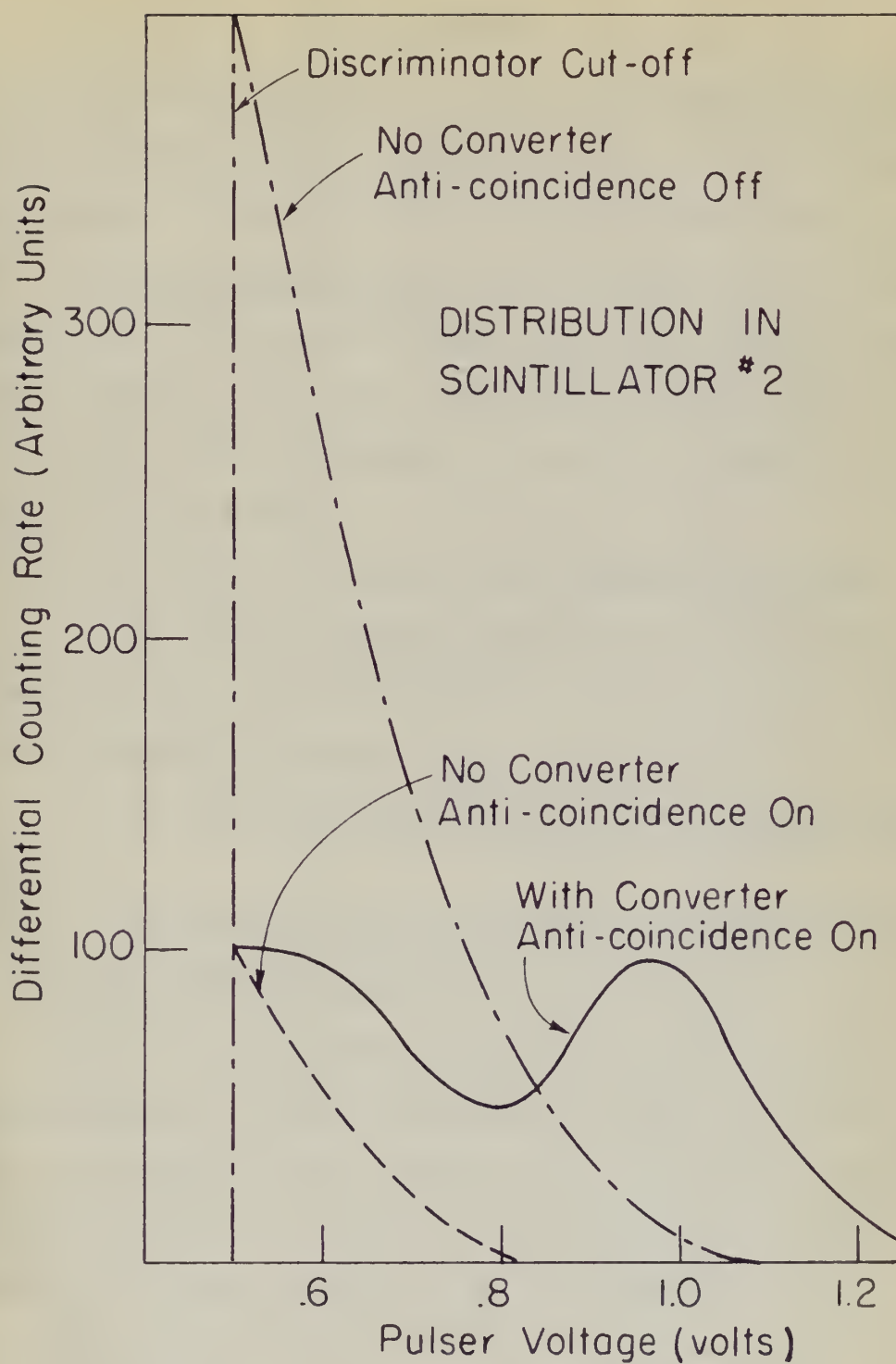
Effect of the Anticoincidence Circuit at 17 Mev
The curves shown were obtained by proton bombardment of a thick lithium metal target, using a 16-mil lead converter. The need for the anticoincidence circuit at high x-ray energy is illustrated.

and many are

The following are the principal results of the investigation. It is found that the rate of reaction is independent of the concentration of the reactants, and that the reaction is first order with respect to the concentration of the catalyst. The rate of reaction is also independent of the temperature, and is not affected by the addition of a large excess of the reactants. The reaction is not affected by the addition of a large excess of the reactants, and is not affected by the addition of a large excess of the reactants.

Figure 17

Effect of the antiozonant on the rate of reaction. The curves shown were obtained by proton bombardment of a thin film of the antiozonant, using a 15-keV beam of protons. The rate of reaction is shown as a function of the antiozonant concentration. The rate of reaction is shown as a function of the antiozonant concentration. The rate of reaction is shown as a function of the antiozonant concentration. The rate of reaction is shown as a function of the antiozonant concentration.



VIII. SUMMARY

An attempt has been made to design, instrument, and calibrate an x-ray scintillation pair spectrometer capable of 10 percent resolution at 10 Mev. The spectrometer is designed for use at the M. I. T. linear accelerator and consequently must span the 5- to 17-Mev x-ray energy region. This three scintillator telescope arrangement relies on the ability of a thin plastic scintillator to distinguish the doubly ionizing pulses originating in the thin lead converter as a result of the pair process.

Careful study of the 6-Mev fluorine gamma-ray has shown:

1. That the observed resolution of 20 to 25 percent is in agreement with predicted values for the thickness of the lead converter and plastic scintillator used;
2. That coincidence pulses are doubly ionizing events, and;
3. Better resolution can be obtained by using a thinner lead converter and thinner plastic scintillator No. 2.

Study of the high-energy incident x-ray region, using the 17-Mev lithium gamma-ray, demonstrated that an anticoincidence circuit was necessary to distinguish doubly ionizing events. Subsequent experimental observations of the pulse height distribution in scintillator No. 2 pointed to the apparent success of the anticoincidence circuit. A program similar to that performed at 6 Mev remains to be carried out at 17 Mev to determine optimum operating conditions in this energy region.

VIII. DISCUSSION

An attempt has been made to design, construct, and calibrate an x-ray scintillation beta spectrometer capable of 10 percent resolution at 10 Mev. The spectrometer is designed for use at the N. I. T. linear accelerator and consequently must span the 2- to 17-Mev x-ray energy region. This poses scintillation detector extremely serious problems. The use of a thin plastic scintillator to distinguish the heavily ionizing pulses originating in the thin lead converter as a result of the beta particles.

General study of the 6-Mev linear gamma-ray has shown:

1. That the observed resolution of 20 to 25 percent is in agreement with predicted values for the thickness of the lead converter and plastic scintillator used;
2. That coincidence pulses are heavily ionizing events;

and;

3. Better resolution can be obtained by using a thinner lead converter and thinner plastic scintillator No. 1.
- Study of the high-energy incident x-ray region, using the 17-Mev linear gamma-ray, demonstrated that an anticoincidence circuit was necessary to distinguish heavily ionizing events. Subsequent experimental observations of the pulse height distribution in scintillator No. 2 pointed to the apparent success of the anticoincidence circuit. A program similar to that performed at 6 Mev remains to be carried out at 17 Mev to determine whether operating conditions in this energy region.

APPENDIX I

CALCULATION OF DIFFERENTIAL ENERGY LOSS DISTRIBUTION FOR SCINTILLATOR No. 2 AT 17.6-Mev INCIDENT X-RAY ENERGY

Using the electron energy distributions given by Johns et al.²⁴ in tabulated form for 1-Mev energy intervals (17.6-Mev incident x-ray energy) and the angular distribution in terms of the electron energy, it is possible to calculate a theoretical energy loss distribution curve for scintillator No. 2 in the following manner. The angle a Compton recoil electron makes with the incident photon is fixed for a given photon energy by the relation²⁵

$$\tan^2 \theta_E = \frac{2\alpha(\gamma/E - 1) - 1}{(1 + \alpha)^2}$$

where γ = energy of incident photon in Mev;

E = energy of recoil electron;

$\alpha = \gamma/mc^2$;

mc^2 = electron rest mass, 0.51 Mev.

The average angle between the direction of motion of a created electron (positive or negative) and of the photon is⁹

$$\theta_0 = \frac{mc^2}{E}$$

where E is the energy of the electron.

二、政治經濟學

RECEIVED
JAN 10 1954
U.S. DEPARTMENT OF AGRICULTURE
WASHINGTON, D.C.

[illegible]

$$\frac{I = (I - 2\sqrt{I})e^{\frac{1}{2}I}}{E_1(I = 1)} = 2\sqrt{I} \cdot e^{\frac{1}{2}I}$$

Once the electron enters the scintillator, it no longer travels in its initial direction given by ϕ_E or θ_0 , but is subjected to single and multiple scattering. One method of finding the actual path length of electrons has been discussed by Yang²⁶. Yang uses a correction Δ such that $t' = t + \Delta$, where t' is the actual path length and t is the foil thickness measured in radiation lengths²⁷.

$$\Delta_{\text{average}} = \frac{t^2 E_s^2}{4P^2 \beta^2},$$

where E_s = characteristic energy = 21.2 Mev;

P = electron momentum in Mev;

β = velocity of electron in units of the velocity of light.

This result was derived from the gaussian approximation of Rossi²⁷ but could be obtained from the exact numerical solution of Snyder and Scott²⁸. It is felt that the gaussian approximation is of reasonable accuracy for these calculations and will be used throughout this paper when investigating multiple scattering effects. Using the above formula and the collision loss as a function of energy given in Johns et al²⁴, it was possible to prepare the histogram shown in Figure 9 for the 17.6-Mev lithium gamma-ray.

The Compton cross section at 17.6 Mev was obtained from Davisson and Evans²⁵; but, since the observed pair production cross sections

Since the electron velocity is infinitesimal, it is no longer
 treated in the initial distribution given by $\delta^3 \mathbf{v}$, but is now
 treated as a single and definite quantity. The method of finding
 the actual path length of electrons has been discussed by Lang²⁴.
 That was a correction δ with time $t' = t + \delta$, where δ is the
 actual path length and t is the full thickness measured in vacuo.
 then $\delta = \frac{v}{c} t$.

$$A_{\text{average}} = \frac{\int_0^t A dt}{\int_0^t dt}$$

where A = instantaneous energy = $E_0 \delta$ (eV)
 δ = electron momentum in eV/c
 v = velocity of electron in units of the velocity of light.

This result was derived from the equation approximation of
 Lang²⁷ but could be obtained from the exact numerical solution of
 Lang²⁸ and Lang²⁹. It is this that the equation approximation is

of reasonable accuracy for these calculations and will be used
 throughout this paper when investigating multiple scattering ef-
 fects. Using the above formula and the collision loss as a func-
 tion of energy given in Table 2, it was possible to improve
 the histogram shown in Figure 2 for the 17.6-MeV electron beam.
 The electron cross section at 17.6 MeV was obtained from Lang³⁰
 and Lang³¹, but since the observed self production cross section

for lead above 5 Mev differ as much as 10 percent from the calculated values, the value for the pair cross section was the experimental value obtained by Waller²⁹.

The energy loss of the electrons in the converter has not been taken into account in any of the curves shown in Figure 9. Hough³⁰ gives the probability of emission at an angle greater than θ_1 (for large angles) as roughly:

$$\frac{3}{8} \left(\frac{mc^2}{E} \right)^2 \frac{1}{1 - \cos \theta_1}$$

where E is the energy of the observed electron. From this, it can be seen that the actual pair angular distribution will spread the energy loss in scintillator No. 2 out towards the higher energy (longer actual path length). The finite resolution of the photomultiplier will spread the distribution out on both sides of the peak. The resulting qualitative curve is shown in Figure 9.

The last three 7 are different as much as 10 percent from the calculated

values, the value for the first error is the experimental

value obtained by Gellert.

The energy loss of the electrons in the experiment has not been

taken into account in any of the curves shown in Figure 2. (Gellert)

From the probability of selection at an angle greater than θ_1 for

large angles, we have

$$\frac{1}{1 - \cos \theta_1} \left(\frac{1}{2} \left(\frac{1}{\sin \theta_1} \right)^2 \right)$$

where θ_1 is the energy of the scattered electron. From this, it can

be seen that the actual value of the probability will exceed the

energy loss in scattering. It is not known the higher energy

(larger angles) is larger. The value of the probability of the

electron will exceed the theoretical one on both sides of the

peak. The resulting calculation curve is shown in Figure 3.

The resulting calculation curve is shown in Figure 3.

The resulting calculation curve is shown in Figure 3.

The resulting calculation curve is shown in Figure 3.

The resulting calculation curve is shown in Figure 3.

The resulting calculation curve is shown in Figure 3.

The resulting calculation curve is shown in Figure 3.

The resulting calculation curve is shown in Figure 3.

BIBLIOGRAPHY

1. H. W. Koch and R. S. Foote, *Phys. Rev.* 91, 455 (1953).
2. J. L. Burkhardt, Ph.D. Thesis, M.I.T., February 1955.
3. H. W. Koch and R. S. Foote, *Rev. Sci. Inst.* 25, 746 (1954).
4. R. L. Walker and B. D. McDaniel, *Phys. Rev.* 74, 315 (1948).
5. B. B. Kinsey and G. A. Bartholomew, *Can. J. Phys.* 31, 537 (1953).
6. R. R. Carlson et al, *Phys. Rev.* 94, 1311 (1954).
7. J. K. Bair and F. C. Maieschein, *Rev. Sci. Inst.* 22, 343 (1951).
8. S. A. E. Johansson, *Nature* 166, 794 (1950); *Phil. Mag.* (London) 43, 249 (1952).
9. Segre, Experimental Nuclear Physics, Vol. I (1953), John Wiley and Sons (New York).
10. R. K. Swank, *Annual Review Nuclear Science* 4, 111 (1954).
11. T. Huus and R. B. Day, *Phys. Rev.* 91, 599 (1953).
12. R. L. Walker, *Phys. Rev.* 79, 172 (1950).
13. H. Mark and G. Goldring, Rockefeller Generator Group, M.I.T., private communication.
14. J. G. Campbell and A. J. F. Boyle, *Australian J. Phys.* 6, 171 (1953).
15. W. Heitler, The Quantum Theory of Radiation, Clarendon Press, Oxford (1936).
16. W. A. Fowler and C. C. Lauritsen, *Phys. Rev.* 76, 314 (1949).
17. C. N. Chou, *Phys. Rev.* 87, 376 (1952).

REFERENCES

1. M. E. Bock and R. E. Thomas, *Phys. Rev.* **81**, 462 (1952).
2. M. E. Bock and R. E. Thomas, *Phys. Rev.* **81**, 462 (1952).
3. M. E. Bock and R. E. Thomas, *Phys. Rev.* **81**, 462 (1952).
4. M. E. Bock and R. E. Thomas, *Phys. Rev.* **81**, 462 (1952).
5. M. E. Bock and R. E. Thomas, *Phys. Rev.* **81**, 462 (1952).
6. M. E. Bock and R. E. Thomas, *Phys. Rev.* **81**, 462 (1952).
7. M. E. Bock and R. E. Thomas, *Phys. Rev.* **81**, 462 (1952).
8. M. E. Bock and R. E. Thomas, *Phys. Rev.* **81**, 462 (1952).
9. M. E. Bock and R. E. Thomas, *Phys. Rev.* **81**, 462 (1952).
10. M. E. Bock and R. E. Thomas, *Phys. Rev.* **81**, 462 (1952).
11. M. E. Bock and R. E. Thomas, *Phys. Rev.* **81**, 462 (1952).
12. M. E. Bock and R. E. Thomas, *Phys. Rev.* **81**, 462 (1952).
13. M. E. Bock and R. E. Thomas, *Phys. Rev.* **81**, 462 (1952).
14. M. E. Bock and R. E. Thomas, *Phys. Rev.* **81**, 462 (1952).
15. M. E. Bock and R. E. Thomas, *Phys. Rev.* **81**, 462 (1952).
16. M. E. Bock and R. E. Thomas, *Phys. Rev.* **81**, 462 (1952).
17. M. E. Bock and R. E. Thomas, *Phys. Rev.* **81**, 462 (1952).

18. L. Katz and A. S. Penfold, *Revs. Modern Phys.* 24, 28 (1952).
19. Pilot Chemical Company, Waltham, Massachusetts.
20. S. Janes, Synchrotron Laboratory, M. I. T., private communication.
21. K. H. Spring, Photons and Electrons, John Wiley and Sons, New York (1950).
22. R. D. Evans, The Atomic Nucleus, McGraw-Hill, to be published.
23. R. M. Sternheimer, *Phys. Rev.* 88, 851 (1952).
24. H. E. Johns et al, *Nucleonics*, 12, 40 (1954).
25. C. M. Davisson and R. D. Evans, *Revs. Modern Phys.* 24, 79 (1952).
26. C. N. Yang, *Phys. Rev.* 84, 599 (1951).
27. B. Rossi and K. Greisen, *Revs. Modern Phys.* 13, 240 (1941).
28. H. Snyder and W. T. Scott, *Phys. Rev.* 76, 220 (1949).
29. R. L. Walker, *Phys. Rev.* 76, 527 (1949).
30. P. V. C. Hough, *Phys. Rev.* 74, 80 (1949).
31. R. K. Swank and W. L. Buck, *Nucleonics* 10-5, 51 (1952).
32. B. R. Linden, *Nucleonics* 11-9, 30 (1953).
33. J. Saldick and A. O. Allen, *J. Chem. Phys.* 22, 438 (1954).
34. H. A. Bethe and W. Heitler, *Proc. Roy. Soc. (London)*, A46, 83 (1934).
35. L. Eyges, *Phys. Rev.* 77, 81 (1950).
36. E. S. Rosenblum, AECU Report No. 1825 (1951).
37. W. Paul and H. Reich, *Z. Physik* 127, 429 (1950).
38. J. J. S. Chen and S. D. Warshaw, *Phys. Rev.* 84, 355 (1951).
39. Goldwasser et al, *Phys. Rev.* 88, 1137 (1952).

18. J. L. Rose and A. D. Henshaw, *Maths*, 1954, 20 (1954).
19. *Mathematical Society, Bulletin*, 1954, 20 (1954).
20. J. L. Rose, *Mathematical Society, Bulletin*, 1954, 20 (1954).
21. J. L. Rose, *Mathematical Society, Bulletin*, 1954, 20 (1954).
22. J. L. Rose, *Mathematical Society, Bulletin*, 1954, 20 (1954).
23. J. L. Rose, *Mathematical Society, Bulletin*, 1954, 20 (1954).
24. J. L. Rose, *Mathematical Society, Bulletin*, 1954, 20 (1954).
25. J. L. Rose, *Mathematical Society, Bulletin*, 1954, 20 (1954).
26. J. L. Rose, *Mathematical Society, Bulletin*, 1954, 20 (1954).
27. J. L. Rose, *Mathematical Society, Bulletin*, 1954, 20 (1954).
28. J. L. Rose, *Mathematical Society, Bulletin*, 1954, 20 (1954).
29. J. L. Rose, *Mathematical Society, Bulletin*, 1954, 20 (1954).
30. J. L. Rose, *Mathematical Society, Bulletin*, 1954, 20 (1954).
31. J. L. Rose, *Mathematical Society, Bulletin*, 1954, 20 (1954).
32. J. L. Rose, *Mathematical Society, Bulletin*, 1954, 20 (1954).
33. J. L. Rose, *Mathematical Society, Bulletin*, 1954, 20 (1954).
34. J. L. Rose, *Mathematical Society, Bulletin*, 1954, 20 (1954).
35. J. L. Rose, *Mathematical Society, Bulletin*, 1954, 20 (1954).
36. J. L. Rose, *Mathematical Society, Bulletin*, 1954, 20 (1954).
37. J. L. Rose, *Mathematical Society, Bulletin*, 1954, 20 (1954).
38. J. L. Rose, *Mathematical Society, Bulletin*, 1954, 20 (1954).
39. J. L. Rose, *Mathematical Society, Bulletin*, 1954, 20 (1954).

40. L. Landau, J. Phys. USSR) 8, 201 (1944).

41. Fano, Nucleonics, 11-8, 8 (1953).

1. The first part of the document is a letter from the author to the editor.

2. The second part is a letter from the editor to the author.

3. The third part is a letter from the author to the editor.

4. The fourth part is a letter from the editor to the author.

5. The fifth part is a letter from the author to the editor.

6. The sixth part is a letter from the editor to the author.

7. The seventh part is a letter from the author to the editor.

8. The eighth part is a letter from the editor to the author.

9. The ninth part is a letter from the author to the editor.

10. The tenth part is a letter from the editor to the author.

11. The eleventh part is a letter from the author to the editor.

12. The twelfth part is a letter from the editor to the author.

13. The thirteenth part is a letter from the author to the editor.

14. The fourteenth part is a letter from the editor to the author.

15. The fifteenth part is a letter from the author to the editor.

16. The sixteenth part is a letter from the editor to the author.

17. The seventeenth part is a letter from the author to the editor.

18. The eighteenth part is a letter from the editor to the author.

19. The nineteenth part is a letter from the author to the editor.

20. The twentieth part is a letter from the editor to the author.

21. The twenty-first part is a letter from the author to the editor.

22. The twenty-second part is a letter from the editor to the author.

23. The twenty-third part is a letter from the author to the editor.

24. The twenty-fourth part is a letter from the editor to the author.

25. The twenty-fifth part is a letter from the author to the editor.



TH 7
S6628

Snyder

28794

Instrumentation and
calibration of X-ray
scintillation pair spectro-
meter.

TH 7
S6628

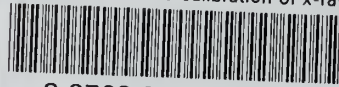
Snyder

28794

Instrumentation and
calibration of X-ray scin-
tillation pair spectrometer.

thesS6628

Instrumentation and calibration of x-ray



3 2768 002 00830 2

DUDLEY KNOX LIBRARY